

**Chaoticity parameter  $\lambda$  in Hanbury-Brown–Twiss interferometry**

Cheuk-Yin Wong\*

*Physics Division, Oak Ridge National Laboratory, Oak Ridge, Tennessee 37831, USA*

Wei-Ning Zhang†

*School of Physics & Optoelectronic Technology, Dalian University of Technology, Dalian 116024, People's Republic of China, and  
Physics Department, Harbin Institute of Technology, Harbin 150006, People's Republic of China*

(Received 2 July 2007; published 27 September 2007)

In Hanbury-Brown–Twiss interferometry measurements using identical bosons, the chaoticity parameter  $\lambda$  has been introduced phenomenologically to represent the momentum correlation function at zero relative momentum. It is useful to study an exactly solvable problem in which the  $\lambda$  parameter and its dependence on the coherence properties of the boson system can be worked out in great detail. We are therefore motivated to study the state of a gas of noninteracting identical bosons at various temperatures held together in a harmonic oscillator potential that arises either externally or from bosons' own mean fields. We determine the degree of Bose-Einstein condensation and its momentum correlation function as a function of the attributes of the boson environment. The parameter  $\lambda$  can then be evaluated from the momentum correlation function. We find that the  $\lambda(p, T)$  parameter is a sensitive function of both the average pair momentum  $p$  and the temperature  $T$ , and the occurrence of  $\lambda = 1$  is not a consistent measure of the absence of a coherent condensate fraction. In particular, for large values of  $p$ , the  $\lambda$  parameter attains the value of unity even for significantly coherent systems with large condensate fractions. We find that if a pion system maintains a static equilibrium within its mean field, and if it contains a root-mean-squared radius, a pion number, and a temperature typical of those in high-energy heavy-ion collisions, then it will contain a large fraction of the Bose-Einstein pion condensate.

DOI: [10.1103/PhysRevC.76.034905](https://doi.org/10.1103/PhysRevC.76.034905)

PACS number(s): 25.75.Gz, 03.75.-b, 05.30.Jp

**I. INTRODUCTION**

In high-energy collision processes, Hanbury-Brown–Twiss (HBT) intensity interferometry [1] has been used to study the space–time geometry of the source of particles [2–38]. As is well known, for identical bosons the interference phenomenon arises from Bose-Einstein correlations and depends sensitively on the degree of coherence of the boson system [39]. The HBT correlation occurs for a chaotic source but not for a coherent source.

In phenomenological measurements, one represents the correlation in terms of the momentum correlation function  $C(\mathbf{p} + \mathbf{q}/2, \mathbf{p} - \mathbf{q}/2) = C(\mathbf{p}_1, \mathbf{p}_2) = G^{(2)}(\mathbf{p}_1, \mathbf{p}_2; \mathbf{p}_1, \mathbf{p}_2) / G^{(1)}(\mathbf{p}_1, \mathbf{p}_1)G^{(1)}(\mathbf{p}_2, \mathbf{p}_2)$ , where  $\mathbf{p}_1$  and  $\mathbf{p}_2$  are the momenta of the pion pair and  $G^{(i)}$  is the  $i$ th-order pion density matrix. One introduces the parameter  $\lambda = [C(q = 0) - 1]$  that is purported to represent the degree of chaoticity of the pion medium and bears the name “the chaoticity parameter.” Experimental measurements with pions persistently indicate that the chaoticity parameter  $\lambda$  is substantially less than the value of unity for a fully chaotic source. Some part of this reduction of the chaoticity parameter  $\lambda$  from unity may be attributed to the occurrence of the decays of long-live resonances [40]. However, as emphasized not the least by Glauber [41], part of the reduction of the chaoticity parameter  $\lambda$  from unity may arise from the coherence of the pion gas.

Even though the chaoticity parameter has been widely used in all HBT measurements in high-energy collisions, how the chaoticity parameter can be determined theoretically has not been resolved. The difficulty is further compounded for heavy-ion collisions because the dynamics of pions after their production in high-energy heavy-ion collisions is very complicated. The process of initial hadronization and the subsequent interactions between pions are beyond the realm of present-day knowledge.

It is therefore useful at this stage to study an exactly solvable problem for which the  $\lambda$  parameter can be determined explicitly and the transition from the coherent phase to the chaotic phase can be worked out in detail. We are motivated to investigate the state of a gas of noninteracting identical bosons held together in a harmonic oscillator potential at various temperatures. We shall study the occurrence of Bose-Einstein condensation and the two-body momentum correlation function as a function of the attributes of the boson gas in such an environment. This will allow us to examine explicitly the transition from the coherent phase to the chaotic phase and to study how this phase transition may affect the HBT measurements and the  $\lambda$  parameter for a set of known attributes of the Bose-Einstein gas assembly.

In atomic physics, the harmonic oscillator potential introduced here can arise from an external trap. In high-energy heavy-ion collisions, the harmonic oscillator potential can arise approximately from the mean-field potential experienced by a pion, owing to the interactions generated by other pions and medium particles. Although the strength of the pion mean field is not known at present, the results obtained here will serve as useful supplementary tools to study the circumstances in

\*wongc@ornl.gov

†wnzhang@dlut.edu.cn

which a pion system may form a Bose-Einstein condensate in heavy-ion collisions. They will stimulate future investigations on the magnitude of the pion mean-field potential and pave the way for future investigations on momentum correlations for pions under more complicated dynamical evolutions.

Pions produced in high-energy heavy-ion collisions have a temperature that is of the order of the pion rest mass. The motion of the pions is relativistic and a proper treatment will need to be relativistic in nature. We shall carry out both a nonrelativistic and a relativistic treatment of the pions to understand what features of the coherence are sensitively affected by the relativistic motion.

Important advances in our understanding of the coherence properties of identical bosons have been made recently in another related field, the physics of atomic boson systems at low temperatures [42–51]. Theoretical and experimental work in atomic physics has focused on the correlation function in the configuration space. In particular, the second-order correlation function  $g^{(2)}(\mathbf{r}_1, \mathbf{r}_2)$  has been obtained to give the probability of detecting a boson at  $\mathbf{r}_1$  in coincidence with the detection of another identical boson at  $\mathbf{r}_2$  [43]. From the shape of this correlation function  $g^{(2)}(\mathbf{r}_1, \mathbf{r}_2)$  as a function of the relative separation  $\mathbf{r}_1 - \mathbf{r}_2$ , the theoretical spatial correlation length can be extracted. Experimentally, the measurements of various arrival times and positions at the detectors in HBT interferometry are then used to determine the spatial correlation length, for comparison with theoretical analyses [50]. We wish to adopt a treatment complementary to that in atomic physics by examining the correlation function in momentum space, the standard arena for Bose-Einstein correlation analysis in high-energy nuclear collisions [2–38]. Our investigation of the correlation function in momentum space is greatly facilitated by utilizing the results of the correlation function in configuration space obtained in atomic physics [42–44].

With regard to the low-temperature measurements with atoms, the perspectives of studying the correlation in momentum space presented here offer useful complementary points of view. In momentum space the trapped atoms are now described as having an equilibrium momentum distribution, appropriate for the system in a given external field at a given temperature. The sudden removal the external field allows the initial momentum distribution of the particle to be frozen at the moment of the external field removal, as appropriate under the application of the sudden approximation in quantum mechanics. Subsequent free streaming of the particles without the external field and mutual interactions allows the reconstruction of the momentum distribution of the source at the moment of its freezing out. In atomic physics, the correlation function in the complementary momentum space has many rich features as it is sensitive to many kinematic variables and the geometry of the source particles.

This paper is organized as follows. In Sec. II, we review the degree of Bose-Einstein condensation as a function of temperature and particle number. In Sec. III, we study the one-body and two-body momentum density matrices. We express the momentum correlation function in terms of the one-body momentum density matrix and the ground-state wave function and also express the momentum correlation function in terms

of the Wigner function in Sec. IV. In Sec. V, we evaluate the one-body density matrix and the Wigner function for bosons in the harmonic oscillator potential. We study the spatial and momentum distributions of these boson assemblies in Sec. VI. In Sec. VII, we evaluate the momentum correlation function  $C(\mathbf{p}, \mathbf{q})$ , for different values of the average pair momentum  $\mathbf{p}$  and temperature  $T$ , and extract the  $\lambda$  parameter and the HBT radii. In Sec. VIII we study the condensate fraction for a nonrelativistic pion gas with a given root-mean-squared radius in static equilibrium at various temperatures. In Sec. IX, we investigate the relativistic treatment of the boson in a harmonic oscillator potential. In Sec. X, we evaluate the boson spatial density and estimate its condensate fraction for the relativistic boson gas. A discussion and our conclusions are presented in Sec. XI.

## II. CONDENSATE FRACTION AS A FUNCTION OF TEMPERATURE

We shall first review the theoretical work on the coherence and correlations of identical bosons in atomic physics [42–44] so as to pave the way for our investigation of the correlation function in momentum space. We consider first a nonrelativistic gas of identical bosons in a harmonic potential at the temperature  $T$  with the potential specified by

$$V(\mathbf{r}) = \frac{1}{2}m\omega^2 r^2 = \frac{1}{2}\hbar\omega \left(\frac{r}{a}\right)^2, \quad (1)$$

where  $m$  is the rest mass of a boson and  $\hbar\omega$  measures the strength of the external potential. We shall measure lengths in units of the harmonic oscillator length parameter  $a = \sqrt{\hbar/m\omega}$ , momenta in units of  $\hbar/a$ , and energies in units of  $\hbar\omega$ .

The states in the harmonic oscillator potential are characterized by energy levels  $\epsilon_n = (n + \frac{3}{2})\hbar\omega$  with the associated degeneracy of  $g_n = (n + 1)(n + 2)/2$ . Following Ref. [43], it is convenient to use the recalibrated energy level  $\tilde{\epsilon}_n = n\hbar\omega$  measured relative to  $3\hbar/2$ .

As the temperature of the gas is lowered below the condensation temperature  $T_c$ , condensation of the nonrelativistic massive boson gas occurs. As is well known, the fluctuation of the number of particles in the condensate state, the  $n = 0$  state, depends sensitively on the assumed statistical ensemble. A grand canonical ensemble will lead to a condensate ground-state number fluctuation that is as large as the number of particles in the condensate ground state,  $n = 0$ . The grand canonical ensemble cannot be used to describe the number of particles,  $N_0$ , in the ground-state condensate. The condensation can best be studied in a canonical ensemble for the case with a fixed number of particles [42]. Comparison of the results from the canonical and the grand canonical ensemble in Ref. [42] indicates however that even though the number of particles in the ground  $n = 0$  state can only be described by the canonical ensemble, the occupation number distribution of the  $n > 0$  harmonic oscillator states can be appropriately described by the grand canonical ensemble with only very small corrections. The difference in these two ensembles for the  $n > 0$  states becomes very small as the number of particles increases.

Therefore, for a fixed number of particles,  $N$ , at a given temperature  $T/\hbar\omega$ , we shall follow Refs. [42] and [43] to determine the condensate configuration by the following requirements: (i) a fixed total number of particles,  $N$ , in a canonical ensemble for the condensate  $n = 0$  state and (ii) an occupation number distribution in a grand canonical ensemble for the  $n > 0$  states. Accordingly, we have the following three conditions to determine the condensate configuration of the system with a fixed number of particles,  $N$ , at a temperature  $T = 1/\beta$ :

$$N = N_0 + N_T, \quad (2)$$

where  $N_0$  is the number of condensate particles in the  $n = 0$  state,

$$N_0 = \frac{z}{1-z}, \quad (3)$$

$N_T$  is the number of ‘‘chaotic’’ particles in the  $n > 0$  states,

$$N_T = \sum_{n>0} \frac{g_n z e^{-\beta \epsilon_n}}{1 - z e^{-\beta \epsilon_n}}, \quad (4)$$

and  $z$  is the fugacity parameter. For the harmonic oscillator potential, the summation for  $N_T$  can be carried out analytically and Eq. (4) can be simplified to

$$N_T = \sum_{k=1}^{\infty} z^k \frac{e^{-k\beta\hbar\omega} (3 - 3e^{-k\beta\hbar\omega} + e^{-2k\beta\hbar\omega})}{(1 - e^{-k\beta\hbar\omega})^3}. \quad (5)$$

Equations (2)–(4) can be reduced into a single condensate configuration condition,

$$N = \frac{z}{1-z} + \sum_{k=1}^{\infty} z^k \frac{e^{-k\beta\hbar\omega} (3 - 3e^{-k\beta\hbar\omega} + e^{-2k\beta\hbar\omega})}{(1 - e^{-k\beta\hbar\omega})^3}. \quad (6)$$

Because  $N$  and  $\beta\hbar\omega = \hbar\omega/T$  are fixed, this condensate configuration condition can be solved numerically to determine the unknown  $z$  (by Newton’s method, with fast convergence). After the value of the solution  $z$  is obtained,  $N_0$  and  $N_T$  can be subsequently determined from Eqs. (3) and (5) to give the condensate configuration specified by the condensate fraction  $f_0$  and the ‘‘chaotic’’ fraction  $f_T$ ,

$$f_0 = \frac{N_0}{N} \quad \text{and} \quad f_T = \frac{N_T}{N}. \quad (7)$$

We show in Fig. 1 the fugacity solution  $z$  that satisfies the condensate configuration condition Eq. (6) for different temperatures  $T/\hbar\omega$  and boson numbers  $N$ . To get a better view of the  $z$  values, we show an expanded view of Fig. 1(a) in the  $z \sim 1$  region in Fig. 1(b). We observe that the fugacity parameter  $z$  is close to unity in the strongly coherent region at low temperatures. In fact, the fugacity parameter  $z$  at  $T = 0$  assumes the value

$$z(T = 0) = \frac{N}{N+1}. \quad (8)$$

For a given boson number  $N$ , as the temperature increases from  $T = 0$ , the fugacity  $z$  decreases very slowly in the form of a plateau until the condensate temperature  $T_c$  is reached, and it decreases very rapidly thereafter. The greater the number of bosons  $N$ , the greater is the plateau region, as shown in

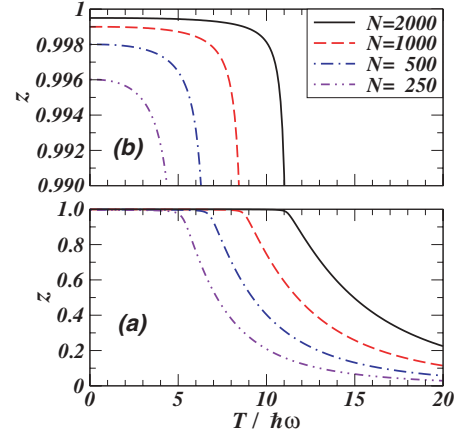


FIG. 1. (Color online) (a) The fugacity parameter  $z$  satisfying the condensate configuration condition Eq. (6) for different boson numbers  $N$ , as a function of the temperature  $T/\hbar\omega$  and (b) an expanded view in the  $z \sim 1$  region.

Fig. 1(b). For example, for  $N = 2000$  the value of  $z$  is close to unity for  $0 < T/\hbar\omega < 11$  in the plateau, and it deviates from unity substantially only for temperatures  $T/\hbar\omega \gg 11$ .

The condensate fractions  $f_0(T)$  calculated with the fugacity parameter of Fig. 1 for different boson numbers  $N$  are represented by solid curves in Fig. 2, as a function of  $T/\hbar\omega$ . The abscissa labels for the corresponding chaotic fraction  $f_T(T) = [1 - f_0(T)]$  are indicated on the right. We observe that the condensate fractions are unity at  $T = 0$ , corresponding to a completely coherent boson system at  $T = 0$ . It decreases slowly as the temperature increases, and the rate of decrease is small at low temperatures. The greater the number of bosons  $N$ , the larger is the range of temperatures in which the boson system contains a substantial fraction of the condensate. For example, for a system with 2000 identical bosons, substantial fraction of the condensate occurs up to  $T/\hbar\omega \sim 11$ . The transition from the condensate phase to the chaotic phase occurs over a large range of temperatures and is therefore not a sharp first-order type transition. The complementary chaotic fraction  $f_T(T)$  increases gradually as the temperature increases, reaching the value of unity at  $T/\hbar\omega \sim 11$  for  $N = 2000$ .

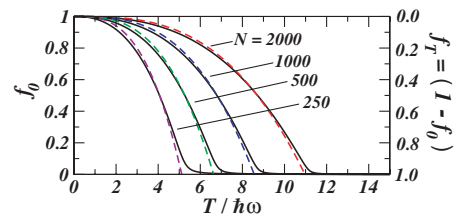


FIG. 2. (Color online) Solid curves represent the condensate fractions  $f_0(T)$ , calculated with the condensate configuration condition Eq. (6), as a function of  $T/\hbar\omega$  for different boson numbers  $N$ . The abscissa labels for the corresponding chaotic fraction  $f_T(T) = [1 - f_0(T)]$  are indicated on the right. The dashed curves are the fits to the solid curve results of  $f_0(T)$  with the function  $1 - (T/T_c)^3$  of Eq. (10), where the values of  $T_c/\hbar\omega$  for different  $N$  values are listed in Table I.

As the number of particles  $N$  decreases down to 250, a substantial condensate fraction occurs only for  $T/\hbar\omega < 5$ . The chaotic fraction  $f_T(T)$  increases as a function of temperature and it reaches the value of unity for  $T/\hbar\omega \sim 6$ . The transition from the condensate phase to the chaotic phase occurs over a temperature range from  $T/\hbar\omega \sim 2$  to  $T/\hbar\omega \sim 5$ . The smaller the number of particles, the lower the condensate temperature  $T_c$  and the smaller is the range of temperatures over which the condensate phase transition occurs.

In the transitional region below  $T_c$  with a substantial fraction of the condensate, one can get an approximate value of the condensate fraction by noting that, in this region, the value of  $z$  is close to unity (Fig. 1). The number of chaotic particles,  $N_T$ , can be estimated from Eq. (5) by setting  $z$  to unity, and we obtain

$$N_T \sim \left(\frac{T}{\hbar\omega}\right)^3 \sum_{k=1}^{\infty} e^{-k\hbar\omega/2T} \left[ \frac{1}{k^3} + \frac{2(\hbar\omega/T)}{k^2} + \frac{15(\hbar\omega/T)^2}{8k} \right]. \quad (9)$$

Consequently, one can fit the condensate fraction  $f_0(T)$  reasonably well by a one-parameter function of the form

$$f_0(T) = 1 - (T/T_c)^3 \quad \text{for } T \leq T_c, \quad (10)$$

$$f_0(T) = O(1/N) \rightarrow 0 \quad \text{for } T \geq T_c. \quad (11)$$

The results from the one-parameter fit to  $f_0(T)$  are shown as the dashed curves in Fig. 2, to be compared with the  $f_0(T)$  calculated with the condensate configuration condition Eq. (6) shown as the solid curves. The values of  $T_c/\hbar\omega$  that give the best fit to  $f_0(T)$  for different  $N$  values are listed in Table I.

The  $T_c$  values can also be determined approximately by considering the case of  $\hbar\omega/T \ll 1$  in Eq. (9), and we have

$$N_T \sim \left(\frac{T}{\hbar\omega}\right)^3 \zeta(3), \quad (12)$$

where  $\zeta(3) = \sum_{k=1}^{\infty} k^{-3} = 1.202$  is the zeta function with the argument 3. Thus, the condensate fraction is given approximately by

$$f_0(T) \sim 1 - (T/T_{c,\text{approx}})^3 \quad \text{for } T < T_{c,\text{approx}}, \quad (13)$$

with

$$\frac{T_{c,\text{approx}}}{\hbar\omega} \sim \left(\frac{N}{\zeta(3)}\right)^{1/3} = \left(\frac{N}{1.202}\right)^{1/3}. \quad (14)$$

A comparison of these approximate result with  $T_c$  in Table I indicates that Eqs. (13) and (14) are approximately valid, with

TABLE I. Condensation temperature  $T_c/\hbar\omega$  of Eq. (10) and  $T_{c,\text{approx}}/\hbar\omega$  of Eq. (14) as a function of  $N$ .

Number of bosons, $N$	$T_c/\hbar\omega$	$T_{c,\text{approx}}/\hbar\omega = (N/1.202)^{1/3}$	$T_{c,\text{approx}}/T_c$
2000	10.97	11.85	1.08
1000	8.56	9.41	1.10
500	6.63	7.47	1.13
250	5.12	5.92	1.16

the values of  $T_{c,\text{approx}}$  determined by Eq. (14) slightly greater than  $T_c$  by about 10%.

### III. ONE-BODY AND TWO-BODY DENSITY MATRICES IN MOMENTUM SPACE

Previously, the one- and two-body density matrices have been obtained for identical bosons in configuration space [43]. We would like to write down the corresponding one-body and two-body density matrices in momentum space so as to evaluate the momentum correlation function. The results in momentum space can be readily obtained from the results in configuration space by replacing  $\mathbf{r}$  in Ref. [43] with  $\mathbf{p}$ . We thus have the one-body density matrix in momentum space

$$G^{(1)}(\mathbf{p}_1, \mathbf{p}_2) = \sum_n u_n^*(\mathbf{p}_1) u_n(\mathbf{p}_2) \langle \hat{a}_n^\dagger \hat{a}_n \rangle. \quad (15)$$

Similarly, we have the two-body density matrix in momentum space given by

$$G^{(2)}(\mathbf{p}_1, \mathbf{p}_2; \mathbf{p}_1, \mathbf{p}_2) = \sum_{klmn} u_k^*(\mathbf{p}_1) u_l^*(\mathbf{p}_2) u_m(\mathbf{p}_2) u_n(\mathbf{p}_1) \times \langle \hat{a}_k^\dagger \hat{a}_l^\dagger \hat{a}_m \hat{a}_n \rangle. \quad (16)$$

We shall follow Ref. [43] in expressing the two-body density matrix in terms of one-body density matrices. By separating out the term with  $k = l = m = n$  from other terms and using the definition of the one-body density matrix (15), the two-body density matrix can be shown to be

$$\begin{aligned} G^{(2)}(\mathbf{p}_1, \mathbf{p}_2; \mathbf{p}_1, \mathbf{p}_2) &= G^{(1)}(\mathbf{p}_1, \mathbf{p}_1) G^{(1)}(\mathbf{p}_2, \mathbf{p}_2) + |G^{(1)}(\mathbf{p}_1, \mathbf{p}_2)|^2 \\ &+ \sum_{n=0}^{\infty} |u_n^*(\mathbf{p}_1)|^2 |u_n(\mathbf{p}_2)|^2 \{ \langle \hat{a}_n^\dagger \hat{a}_n^\dagger \hat{a}_n \hat{a}_n \rangle \\ &- 2 \langle \hat{a}_n^\dagger \hat{a}_n \rangle \langle \hat{a}_n^\dagger \hat{a}_n \rangle \}. \end{aligned} \quad (17)$$

The last term in this equation involves a summation over the  $n = 0$  condensate state and the set of  $\{n > 0\}$  states. In line with our earlier discussions on the statistical ensemble for the states [42,43], we shall use the grand canonical ensemble for the set of  $\{n > 0\}$  states and the canonical ensemble for the condensate state of  $n = 0$ . For the set of  $\{n > 0\}$  states in the grand canonical ensemble then, the occupation fluctuation characteristics of the grand canonical ensemble make the contributions of the set of  $\{n > 0\}$  states small in comparison with the other terms on the right-hand side of Eq. (17), as we shall see from the following discussion. We note that in this equation

$$\begin{aligned} &\langle \hat{a}_n^\dagger \hat{a}_n^\dagger \hat{a}_n \hat{a}_n \rangle - 2 \langle \hat{a}_n^\dagger \hat{a}_n \rangle \langle \hat{a}_n^\dagger \hat{a}_n \rangle \\ &= \langle (\hat{a}_n^\dagger \hat{a}_n - \langle \hat{a}_n^\dagger \hat{a}_n \rangle)^2 \rangle - \langle \hat{a}_n^\dagger \hat{a}_n \rangle \langle \hat{a}_n^\dagger \hat{a}_n \rangle. \end{aligned} \quad (18)$$

For an  $n > 0$  state in the grand canonical ensemble, the mean-square fluctuation of the occupation number  $\langle \hat{a}_n^\dagger \hat{a}_n \rangle$  in the state is given by [52]

$$\langle (\hat{a}_n^\dagger \hat{a}_n - \langle \hat{a}_n^\dagger \hat{a}_n \rangle)^2 \rangle = \langle \hat{a}_n^\dagger \hat{a}_n \rangle (\langle \hat{a}_n^\dagger \hat{a}_n \rangle + 1). \quad (19)$$

Therefore, for this  $n > 0$  state in the grand canonical ensemble, we have

$$\langle \hat{a}_n^\dagger \hat{a}_n^\dagger \hat{a}_n \hat{a}_n \rangle - 2 \langle \hat{a}_n^\dagger \hat{a}_n \rangle \langle \hat{a}_n^\dagger \hat{a}_n \rangle = \langle \hat{a}_n^\dagger \hat{a}_n \rangle, \quad (20)$$

and the contribution of the set of  $\{n > 0\}$  states to the two-body density matrix is

$$\sum_{n>0} |u_n^*(\mathbf{p}_1)|^2 |u_n(\mathbf{p}_2)|^2 \langle \hat{a}_n^\dagger \hat{a}_n \rangle. \quad (21)$$

When we integrate over  $\mathbf{p}_1$  and  $\mathbf{p}_2$ , the set of  $\{n > 0\}$  states gives a contribution of

$$\int d\mathbf{p}_1 d\mathbf{p}_2 \sum_{n>0} |u_n^*(\mathbf{p}_1)|^2 |u_n(\mathbf{p}_2)|^2 \langle \hat{a}_n^\dagger \hat{a}_n \rangle = N_T, \quad (22)$$

whereas the other terms, such as the first term of Eq. (17),  $G^{(1)}(\mathbf{p}_1, \mathbf{p}_1)G^{(1)}(\mathbf{p}_2, \mathbf{p}_2)$ , give a contribution of  $N^2$ . The contribution from the set of  $\{n > 0\}$  states is  $N_T/N^2$  of the contribution from  $G^{(1)}(\mathbf{p}_1, \mathbf{p}_1)G^{(1)}(\mathbf{p}_2, \mathbf{p}_2)$ . Therefore, in the limit of a large number of bosons,  $N$ , the ratio  $N_T/N^2$  is small, and the contributions from the set of  $\{n > 0\}$  states in the summation in Eq. (17) can be neglected. We are left with only the  $n = 0$  condensate state contribution for this summation.

To describe the  $n = 0$  condensate state, we shall follow Refs. [42,43] and use the canonical ensemble, which gives the canonical fluctuation [42]

$$\langle (\hat{a}_n^\dagger \hat{a}_n - \langle \hat{a}_n^\dagger \hat{a}_n \rangle)^2 \rangle = \langle \hat{a}_0^\dagger \hat{a}_0^\dagger \hat{a}_0 \hat{a}_0 \rangle - \langle \hat{a}_0^\dagger \hat{a}_0 \rangle \langle \hat{a}_0^\dagger \hat{a}_0 \rangle = O(N_0). \quad (23)$$

Thus, we have

$$\langle \hat{a}_n^\dagger \hat{a}_n^\dagger \hat{a}_n \hat{a}_n \rangle - 2 \langle \hat{a}_n^\dagger \hat{a}_n \rangle \langle \hat{a}_n^\dagger \hat{a}_n \rangle = -\langle \hat{a}_0^\dagger \hat{a}_0 \rangle \langle \hat{a}_0^\dagger \hat{a}_0 \rangle + O(N_0). \quad (24)$$

In the limit of a large number of particles, we can neglect the last term  $O(N_0)$  in this equation, which is small compared to the first term of order  $N_0^2$ . The two-body momentum density matrix of Eq. (17) is therefore

$$\begin{aligned} G^{(2)}(\mathbf{p}_1, \mathbf{p}_2; \mathbf{p}_1, \mathbf{p}_2) \\ = G^{(1)}(\mathbf{p}_1, \mathbf{p}_1)G^{(1)}(\mathbf{p}_2, \mathbf{p}_2) + |G^{(1)}(\mathbf{p}_1, \mathbf{p}_2)|^2 \\ - N_0^2 |u_0(\mathbf{p}_1)|^2 |u_0(\mathbf{p}_2)|^2, \end{aligned} \quad (25)$$

which gives the conditional probability for the occurrence of a pion of momentum  $\mathbf{p}_1$  in coincidence with another identical pion of momentum  $\mathbf{p}_2$ . This two-body density matrix in momentum space has the same form as that obtained earlier in configuration space in Ref. [43].

#### IV. THE MOMENTUM CORRELATION FUNCTION

In HBT measurements, we normalize the probability relative to the probability of detecting particle  $\mathbf{p}_1$  and  $\mathbf{p}_2$ , and we define the momentum correlation function  $C(\mathbf{p}_1, \mathbf{p}_2)$  as

$$C(\mathbf{p}_1, \mathbf{p}_2) = \frac{G^{(2)}(\mathbf{p}_1, \mathbf{p}_2; \mathbf{p}_1, \mathbf{p}_2)}{G^{(1)}(\mathbf{p}_1, \mathbf{p}_1)G^{(1)}(\mathbf{p}_2, \mathbf{p}_2)}. \quad (26)$$

It is convenient to introduce the average and the relative momenta of the pair,

$$\mathbf{p} = (\mathbf{p}_1 + \mathbf{p}_2)/2, \quad \mathbf{q} = \mathbf{p}_1 - \mathbf{p}_2, \quad (27)$$

with the inverse transformation

$$\mathbf{p}_1 = \mathbf{p} + \frac{\mathbf{q}}{2}, \quad \mathbf{p}_2 = \mathbf{p} - \frac{\mathbf{q}}{2}. \quad (28)$$

The momentum correlation function can be expressed alternatively in terms of the kinematic variables  $\mathbf{p}$  and  $\mathbf{q}$ . From Eq. (25), we have the general expression for the correlation function

$$\begin{aligned} C(\mathbf{p}, \mathbf{q}) &= C(\mathbf{p}_1, \mathbf{p}_2) \\ &= 1 + \frac{|G^{(1)}(\mathbf{p}_1, \mathbf{p}_2)|^2 - N_0^2 |u_0(\mathbf{p}_1)|^2 |u_0(\mathbf{p}_2)|^2}{G^{(1)}(\mathbf{p}_1, \mathbf{p}_1)G^{(1)}(\mathbf{p}_2, \mathbf{p}_2)}. \end{aligned} \quad (29)$$

In the nearly completely coherent case with almost all particles in the ground condensate state,  $N_0 \rightarrow N$ , the two terms in the numerator cancel each other and we have  $C(p, q) = 1$ , as it should be. For the other extreme of a completely chaotic source with  $N_0 \ll N$ , the second term in the numerator proportional to  $N_0^2$  gives negligible contribution and can be neglected. The correlation function becomes the usual one for a completely chaotic source,

$$C_{\text{chaotic}}(\mathbf{p}, \mathbf{q}) = 1 + \frac{|G^{(1)}(\mathbf{p}_1, \mathbf{p}_2)|^2}{G^{(1)}(\mathbf{p}_1, \mathbf{p}_1)G^{(1)}(\mathbf{p}_2, \mathbf{p}_2)}. \quad (30)$$

The general result of Eq. (29) allows one to study the correlation function for all cases with varying degrees of coherence.

If we introduce  $R(\mathbf{p}, \mathbf{q}) = R(\mathbf{p}_1, \mathbf{p}_1) = C(\mathbf{p}, \mathbf{q}) - 1$ , then

$$\begin{aligned} R(\mathbf{p}, \mathbf{q}) &= R(\mathbf{p}_1, \mathbf{p}_2) \\ &= \frac{|G^{(1)}(\mathbf{p}_1, \mathbf{p}_2)|^2 - N_0^2 |u_0(\mathbf{p}_1)|^2 |u_0(\mathbf{p}_2)|^2}{G^{(1)}(\mathbf{p}_1, \mathbf{p}_1)G^{(1)}(\mathbf{p}_2, \mathbf{p}_2)}. \end{aligned} \quad (31)$$

It is of interest to express the momentum correlation function  $C(p, q)$  in terms of the Wigner function  $f(\mathbf{r}, \mathbf{p})$  defined in terms of the one-body density matrix  $G^{(1)}(\mathbf{r}_1, \mathbf{r}_2)$  as

$$f(\mathbf{r}, \mathbf{p}) = \int ds e^{i\mathbf{p}\cdot\mathbf{s}} G^{(1)}\left(\mathbf{r} + \frac{\mathbf{s}}{2}, \mathbf{r} - \frac{\mathbf{s}}{2}\right). \quad (32)$$

This one-body density matrix in configurations space is related to the one-body density matrix in momentum space by a Fourier transform,

$$G^{(1)}(\mathbf{p}_1, \mathbf{p}_2) = \int d\mathbf{r}_1 d\mathbf{r}_2 e^{i\mathbf{p}_1\cdot\mathbf{r}_1 - i\mathbf{p}_2\cdot\mathbf{r}_2} G^{(1)}(\mathbf{r}_1, \mathbf{r}_2). \quad (33)$$

Therefore, by changing coordinates from  $\mathbf{r}_1$  and  $\mathbf{r}_2$  to  $\mathbf{r} = (\mathbf{r}_1 + \mathbf{r}_2)/2$  and  $\mathbf{s} = \mathbf{r}_1 - \mathbf{r}_2$ , we can relate the one-body density  $G^{(1)}(\mathbf{p}_1, \mathbf{p}_2)$  with the Wigner function  $f(\mathbf{r}, \mathbf{p})$ ,

$$G^{(1)}(\mathbf{p}_1, \mathbf{p}_2) = \int d\mathbf{r} e^{i\mathbf{q}\cdot\mathbf{r}} f(\mathbf{r}, \mathbf{p}), \quad (34)$$

and, in particular, for the diagonal density matrix element we have

$$G^{(1)}(\mathbf{p}_1, \mathbf{p}_1) = \int d\mathbf{r} f(\mathbf{r}, \mathbf{p}_1). \quad (35)$$

$$C(\mathbf{p}, \mathbf{q}) = 1 + \frac{|\int d\mathbf{r} e^{i\mathbf{q}\cdot\mathbf{r}} f(\mathbf{r}, \mathbf{p})|^2 - N_0^2 |u_0(\mathbf{p} + \mathbf{q}/2)|^2 |u_0(\mathbf{p} - \mathbf{q}/2)|^2}{\int d\mathbf{r} f(\mathbf{r}, \mathbf{p} + \mathbf{q}/2) \int d\mathbf{r} f(\mathbf{r}, \mathbf{p} - \mathbf{q}/2)}. \quad (36)$$

This is the general expression for the momentum correlation function expressed in terms of the Wigner function  $f(\mathbf{r}, \mathbf{p})$  when the coherence of the system is properly taken into account.

The  $R$  function for the general case is related to the Wigner function  $f(\mathbf{r}, \mathbf{p})$  by

$$\begin{aligned} R(\mathbf{p}, \mathbf{q}) &= \frac{|\int d\mathbf{r} e^{i\mathbf{q}\cdot\mathbf{r}} f(\mathbf{r}, \mathbf{p})|^2 - N_0^2 |u_0(\mathbf{p} + \mathbf{q}/2)|^2 |u_0(\mathbf{p} - \mathbf{q}/2)|^2}{\int d\mathbf{r} f(\mathbf{r}, \mathbf{p} + \mathbf{q}/2) \int d\mathbf{r} f(\mathbf{r}, \mathbf{p} - \mathbf{q}/2)}. \end{aligned} \quad (37)$$

When the condensate fraction  $f_0$  is large with  $N_0 \rightarrow N$ , the second term in the numerator of this equations is important and must be properly taken into account. In fact, in the completely coherent case, Eqs. (36) and (37) give  $C(p, q) = 1$  and  $R(p, q) = 0$ . Only in the special case of a completely chaotic state is the contribution from the second term in the numerator negligible, and we have the usual relationship between the Wigner function and the momentum correlation function for a chaotic system,

$$C_{\text{chaotic}}(\mathbf{p}, \mathbf{q}) \sim 1 + \frac{|\int d\mathbf{r} e^{i\mathbf{q}\cdot\mathbf{r}} f(\mathbf{r}, \mathbf{p})|^2}{\int d\mathbf{r} f(\mathbf{r}, \mathbf{p} + \mathbf{q}/2) \int d\mathbf{r} f(\mathbf{r}, \mathbf{p} - \mathbf{q}/2)}. \quad (38)$$

## V. THE ONE-BODY DENSITY MATRIX FOR A HARMONIC OSCILLATOR POTENTIAL

For a given total particle number  $N$  of particle mass  $m$  in an external harmonic oscillator potential, we have obtained in Sec. II the fugacity  $z$  as a function of  $T/\hbar\omega$  (Fig. 1). This solution of  $z$  allows us to evaluate the density matrices and the correlation functions at various temperatures. For the harmonic oscillator potential, the one-body density matrix has been obtained previously in configuration space as given by [43]

$$\begin{aligned} G^{(1)}(\mathbf{r}_1, \mathbf{r}_2) &= \sum_{n=0}^{\infty} u_n^*(\mathbf{r}_1) u_n(\mathbf{r}_2) \frac{z e^{-\beta \tilde{\epsilon}_n}}{1 - z e^{-\beta \tilde{\epsilon}_n}} \\ &= \sum_{k=1}^{\infty} z^k \tilde{G}_0(\mathbf{r}_1, \mathbf{r}_2; k\beta\hbar\omega), \end{aligned} \quad (39)$$

where

$$\begin{aligned} \tilde{G}_0(\mathbf{r}_1, \mathbf{r}_2; \tau) &= \left( \frac{1}{\pi a^2 (1 - e^{-2\tau})} \right)^{3/2} \\ &\times \exp \left( -\frac{1}{a^2} \frac{(\mathbf{r}_1^2 + \mathbf{r}_2^2) (\cosh \tau - 1) + (\mathbf{r}_1 - \mathbf{r}_2)^2}{2 \sinh \tau} \right). \end{aligned} \quad (40)$$

Because of the exchange symmetry of  $\mathbf{r}/a$  and  $\mathbf{p}a/\hbar$  for a harmonic oscillator potential, the one-body density matrix in momentum space can be readily obtained from these results of Ref. [43] by replacing  $\mathbf{r}/a$  with  $\mathbf{p}a/\hbar$ , and we get

$$\begin{aligned} G^{(1)}(\mathbf{p}_1, \mathbf{p}_2) &= \sum_{n=0}^{\infty} u_n^*(\mathbf{p}_1) u_n(\mathbf{p}_2) \frac{z e^{-\beta \tilde{\epsilon}_n}}{1 - z e^{-\beta \tilde{\epsilon}_n}} \\ &= \sum_{k=1}^{\infty} z^k \tilde{G}_0(\mathbf{p}_1, \mathbf{p}_2; k\beta\hbar\omega), \end{aligned} \quad (41)$$

where

$$\begin{aligned} \tilde{G}_0(\mathbf{p}_1, \mathbf{p}_2; \tau) &= \left( \frac{a^2}{\pi \hbar^2 (1 - e^{-2\tau})} \right)^{3/2} \\ &\times \exp \left( -\frac{a^2 (\mathbf{p}_1^2 + \mathbf{p}_2^2) (\cosh \tau - 1) + (\mathbf{p}_1 - \mathbf{p}_2)^2}{\hbar^2 2 \sinh \tau} \right). \end{aligned} \quad (42)$$

We can write  $\tilde{G}_0(\mathbf{p}_1, \mathbf{p}_2; \tau)$  in terms of the ground-state wave function  $u_0^*(\mathbf{p}_1) u_0(\mathbf{p}_2)$  as

$$\tilde{G}_0(\mathbf{p}_1, \mathbf{p}_2; \tau) = u_0^*(\mathbf{p}_1) u_0(\mathbf{p}_2) \tilde{g}_0(\mathbf{p}_1, \mathbf{p}_2; \tau), \quad (43)$$

where the ground-state wave function is

$$u_0(\mathbf{p}) = \left( \frac{a^2}{\pi \hbar^2} \right)^{3/4} \exp \left\{ -\frac{a^2 \mathbf{p}^2}{\hbar^2 2} \right\}, \quad (44)$$

and the dimensionless function  $\tilde{g}_0(\mathbf{p}_1, \mathbf{p}_2; \tau)$  is given by

$$\begin{aligned} \tilde{g}_0(\mathbf{p}_1, \mathbf{p}_2; \tau) &= \frac{1}{(1 - e^{-2\tau})^{3/2}} \\ &\exp \left( -\frac{a^2 (\mathbf{p}_1^2 + \mathbf{p}_2^2) (\cosh \tau - 1 - \sinh \tau) + (\mathbf{p}_1 - \mathbf{p}_2)^2}{\hbar^2 2 \sinh \tau} \right). \end{aligned} \quad (45)$$

Then we have

$$G^{(1)}(\mathbf{p}_1, \mathbf{p}_2) = u_0^*(\mathbf{p}_1) u_0(\mathbf{p}_2) A(\mathbf{p}_1, \mathbf{p}_2), \quad (46)$$

where

$$A(\mathbf{p}_1, \mathbf{p}_2) = \sum_{k=1}^{\infty} z^k \tilde{g}_0(\mathbf{p}_1, \mathbf{p}_1; k\beta\hbar\omega). \quad (47)$$

In numerical calculations, especially at low temperatures where  $z$  is close to unity, the number of terms in the summation over  $k$  in  $A(\mathbf{p}_1, \mathbf{p}_2)$  will need to be greater than the number of particles,  $N$ . To avoid such a lengthy summation, it is simplest to separate out the condensate component to write Eq. (47) as

$$A(\mathbf{p}_1, \mathbf{p}_2) = \frac{z}{1 - z} + \sum_{k=1}^{\infty} z^k [\tilde{g}_0(\mathbf{p}_1, \mathbf{p}_1; k\beta\hbar\omega) - 1]. \quad (48)$$

For low temperatures, the coefficient  $[\tilde{g}_0(\mathbf{p}_1, \mathbf{p}_1; k\beta\hbar\omega) - 1]$  of  $z^k$  is small and a small number of terms in  $k$  will suffice. For high temperatures above the condensate temperature,  $z$  is substantially less than unity, and  $z^k$  decreases rapidly as  $k$  increases; a small number of terms in  $k$  will also suffice.

From Eq. (29) the momentum correlation function is

$$C(\mathbf{p}, \mathbf{q}) = C(\mathbf{p}_1, \mathbf{p}_2) = 1 + \frac{|A(\mathbf{p}_1, \mathbf{p}_2)|^2 - |z/(1-z)|^2}{A(\mathbf{p}_1, \mathbf{p}_1)A(\mathbf{p}_2, \mathbf{p}_2)} \quad (49)$$

and

$$R(\mathbf{p}, \mathbf{q}) = R(\mathbf{p}_1, \mathbf{p}_2) = \frac{|A(\mathbf{p}_1, \mathbf{p}_2)|^2 - |z/(1-z)|^2}{A(\mathbf{p}_1, \mathbf{p}_1)A(\mathbf{p}_2, \mathbf{p}_2)}. \quad (50)$$

The one-body Wigner function for the boson system can be obtained from the one-body density matrix  $G^{(1)}(\mathbf{r}_1, \mathbf{r}_2)$  and we find

$$f(\mathbf{r}, \mathbf{p}) = \sum_{k=1}^{\infty} z^k \left( \frac{4 \tanh(k\beta\hbar\omega/2)}{(1 - e^{-2k\beta\hbar\omega})} \right)^{3/2} \times \exp \left[ - \left( \frac{r^2}{a^2} + \frac{\mathbf{p}^2 a^2}{\hbar^2} \right) \tanh \left( \frac{k\beta\hbar\omega}{2} \right) \right]. \quad (51)$$

There is an explicit symmetry between  $\mathbf{x}/a$  and  $\mathbf{p}a$  in the Wigner function for the harmonic oscillator potential.

## VI. SPATIAL AND MOMENTUM DISTRIBUTIONS

Before we evaluate the momentum correlation function  $C(p, q)$ , it is useful to study the single-particle spatial and momentum distributions  $\rho_r(\mathbf{r})$  and  $\rho_p(\mathbf{p})$ . Because of the symmetry between  $\mathbf{r}/a$  and  $\mathbf{p}a/\hbar$  in a harmonic oscillator potential, the following two functions have the same shape: (i)  $\rho_r(\mathbf{r})$  in units of  $a^{-3}$  expressed as a function of  $\mathbf{r}/a$  and (ii)  $\rho_p(\mathbf{p})$  in units of  $(a/\hbar)^3$  expressed as a function of  $\mathbf{p}a/\hbar$ . The two distributions can be displayed on the same graph. From the one-body density matrix (46), we obtain

$$\rho_p(\mathbf{p}) = G^{(1)}(\mathbf{p}, \mathbf{p}) = \left( \frac{a^2}{\pi\hbar^2} \right)^{3/2} \exp \left( - \frac{a^2 \mathbf{p}^2}{\hbar^2} \right) A(\mathbf{p}, \mathbf{p}), \quad (52)$$

where

$$A(\mathbf{p}, \mathbf{p}) = \sum_{k=1}^{\infty} z^k \tilde{g}_0(\mathbf{p}, \mathbf{p}; k\beta\hbar\omega), \quad (53)$$

$$\tilde{g}_0(\mathbf{p}, \mathbf{p}; \tau) = \frac{1}{(1 - e^{-2\tau})^{3/2}} \times \exp \left( - \frac{a^2 \mathbf{p}^2 (\cosh \tau - 1 - \sinh \tau)}{\hbar^2 \sinh \tau} \right). \quad (54)$$

We plot in Fig. 3 the spatial and momentum distributions of the system with  $N = 2000$  as a function of their dimensionless variables  $r/a$  and  $pa/\hbar$ , respectively. One observes that up to  $T/\hbar\omega \sim 9$  the system has a small spatial or momentum size

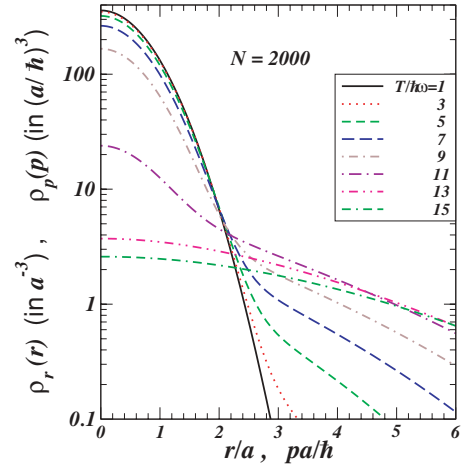


FIG. 3. (Color online) The spatial density distribution  $\rho_r(\mathbf{r})$  in units of  $a^{-3}$ , expressed as a function of  $r/a$ , and the momentum density distribution  $\rho_p(\mathbf{p})$  in units of  $(a/\hbar)^3$ , expressed as a function of  $pa/\hbar$ , for a boson system with  $N = 2000$  at different temperatures.

and there is a substantial condensate fraction in the system. In Fig. 4 we plot the root-mean-squared radius in units of  $a$ ,  $r_{\text{rms}}/a = \sqrt{\langle (r/a)^2 \rangle}$ , and the root-mean-squared momentum in units of  $\hbar/a$ ,  $p_{\text{rms}}a/\hbar = \sqrt{\langle (pa/\hbar)^2 \rangle}$ , as a function of  $T/\hbar\omega$ . For  $N = 2000$ , the quantity  $r_{\text{rms}}/a$  is slightly greater than 1 up to  $T/\hbar\omega \sim 6$ , and it increases relatively rapidly to about 5.5 at the condensate temperature,  $T_c/\hbar\omega \sim 11$ . It increases at a relatively slower rate at temperatures above  $T_c$ .

The size of the momentum distribution also undergoes similar changes as a function of temperature. The root-mean-squared momentum has the dimension of about one unit of  $\hbar/a$  at  $T/\hbar\omega \sim 0$  and this linear size increases about sixfold when the temperature reaches the chaotic region of  $T_c/\hbar\omega \sim 11$  for  $N = 2000$ .

We observe therefore that, for a boson system in a harmonic oscillator, the Bose-Einstein condensation gives rise to a distribution localized in the region of small momentum and small spatial coordinates. From the viewpoints of the spatial and momentum densities, the Bose-Einstein condensate in

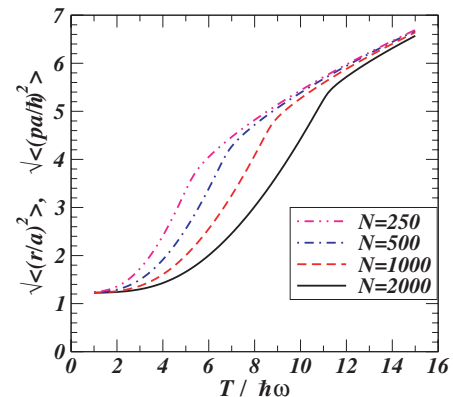


FIG. 4. (Color online) The root-mean-squared radius in unit of  $a$  and the root-mean-squared momentum in units of  $\hbar/a$ , as a function of  $T/\hbar\omega$  for different numbers of bosons in the system.

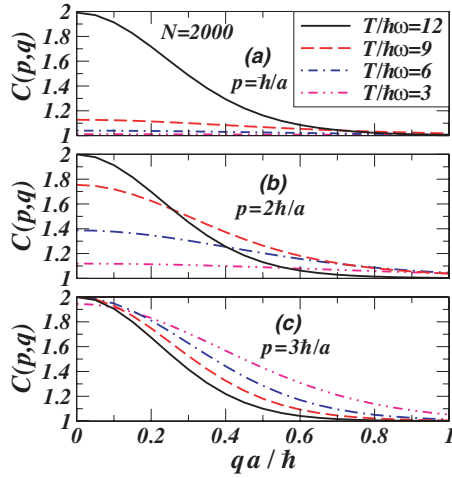


FIG. 5. (Color online) The correlation function at different values of the pair momentum  $pa/\hbar$  and temperatures. Panels (a), (b), and (c) are for  $p = 1, 2,$  and  $3\hbar/a$ , respectively.

a harmonic oscillator is therefore a “condensation” in both momentum space and configuration space.

## VII. EVALUATION OF THE MOMENTUM CORRELATION FUNCTION $C(p, q)$

With the solution  $z$  obtained for a given  $T/\hbar\omega$  as shown in Fig. 1 and discussed in Sec. II, one can use Eq. (48) to evaluate  $A(\mathbf{p}_1, \mathbf{p}_2)$ . The knowledge of  $A(\mathbf{p}_1, \mathbf{p}_2)$  then allows the determination of the momentum correlation function from  $C(p, q)$  using Eq. (49).

We show results of  $C(p, q)$  for the case of  $N = 2000$  in Fig. 5. We observe that the correlation function is a complicated function of the average pair momentum  $p$  and the temperature  $T$ . For  $p = \hbar/a$  in Fig. 5(a), the correlation function  $C(p, q)$  at  $q = 0$  is close to unity for temperatures below and up to  $T/\hbar\omega = 9$ , but it increases to 2 rather abruptly at  $T/\hbar\omega = 12$ . For  $p = 2\hbar/a$  in Fig. 5(b), the correlation function  $C(p, q)$  at  $q = 0$  is substantially above unity and increases gradually as temperature increases. For  $p = 3\hbar/a$  in Fig. 5(c), the correlation function  $C(p, q)$  at  $q = 0$  is about 2 for all temperatures examined.

If one follows the standard phenomenological analysis and introduces the chaoticity parameter  $\lambda$  to represent the correlation function at zero relative momentum, then this parameter  $\lambda$  is a function of the average pair momentum  $p$  and the temperature  $T$ :

$$\lambda(p, T) = [C(p, q = 0; T) - 1], \quad (55)$$

where we display explicitly the dependence of the correlation function on the temperature  $T$ . We plot the values of  $\lambda(p, T)$  as a function of  $p$  in Fig. 6(a) for different temperatures for the case of  $N = 2000$ . At  $T/\hbar\omega = 12$ , which is above the condensate temperature  $T_c$ , the  $\lambda$  parameter is 1 for all  $p$  values. At  $T/\hbar\omega = 9$ , which is below the condensate temperature  $T_c$ , the  $\lambda$  parameter drops precipitously to  $\sim 0.1$  at  $pa/\hbar = 1$ . At this  $T/\hbar\omega = 9$ , as  $p$  increases the  $\lambda$  parameter rises gradually and reaches the constant value of 1 at  $pa/\hbar = 2.4$ . At  $T/\hbar\omega =$

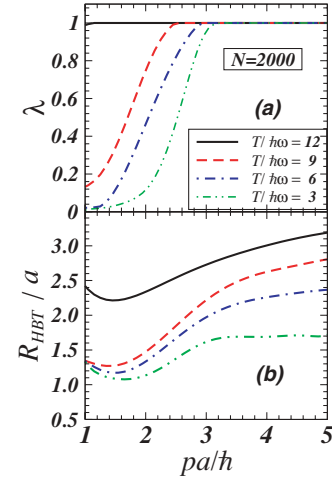


FIG. 6. (Color Online) (a) The parameter  $\lambda$  as a function of  $pa/\hbar$  for different temperatures for  $N = 2000$ . (b) The ratio  $R_{\text{HBT}}/a$  as a function of  $pa/\hbar$  for different temperatures for  $N = 2000$ .

6 and 3, for which the systems are significantly coherent with large condensate fractions, the  $\lambda$  parameter starts close to zero at  $pa/\hbar = 1$ , but as  $p$  increases the  $\lambda$  parameter increases gradually to unity at  $pa/\hbar = 2.9$  and  $3.1$  for  $T/\hbar\omega = 6$  and  $3$ , respectively. The location where the  $\lambda$  parameter attains unity changes with temperature. The lower the temperature, the greater is the value of  $p$  at which the  $\lambda$  parameter attains unity.

We conclude from our results that the parameter  $\lambda(p, T)$  is a sensitive function of both  $p$  and  $T$  and  $\lambda(p, T) = 1$  is not a consistent measure of the absence of the condensate fraction, as it attains the value of unity in some kinematic regions for significantly coherent systems with large condensate fractions at temperatures much below  $T_c$ . Only for the region of small  $p$  will the parameter  $\lambda(p, T)$  be correlated with, but not equal to, the chaotic fraction  $f_T(T)$  of the system.

One can evaluate the root-mean-squared momentum in the correlation function defined as

$$q_{\text{rms}}^2(p, T) = \langle q^2 \rangle = \frac{\int d\mathbf{q} q^2 [C(p, q; T) - 1]}{\int d\mathbf{q} [C(p, q; T) - 1]} \quad (56)$$

and introduce the HBT radius  $R_{\text{HBT}}(p, T)$  defined by

$$R_{\text{HBT}}(p, T) = \sqrt{\frac{3}{2}} \frac{\hbar}{q_{\text{rms}}(p, T)}. \quad (57)$$

The HBT radius  $R_{\text{HBT}}(p, T)$  is in fact the radius parameter in the standard Gaussian parametrization of the momentum correlation function,

$$C(p, q; T) = 1 + \lambda(p, T) \exp[-q^2 R_{\text{HBT}}^2(p, T)/\hbar^2]. \quad (58)$$

We plot  $R_{\text{HBT}}(p, T)$  as a function of  $pa/\hbar$  for different temperatures  $T$  for the case of  $N = 2000$  in Fig. 6(b). For fixed values of the temperature  $T/\hbar\omega = 3, 6,$  and  $9$  and varying  $p$ , one observes that  $R_{\text{HBT}}(p, T)$  is about  $1.3a$  and  $R_{\text{HBT}}(p, T)$  decreases slightly before it increases gradually as  $p$  increases. For  $T/\hbar\omega = 12$ , which is above the condensate temperature,  $R_{\text{HBT}}(p, T)$  is about  $2.4a$  at  $pa/\hbar = 1$ , and  $R_{\text{HBT}}(p, T)$  decreases slightly before it increases gradually

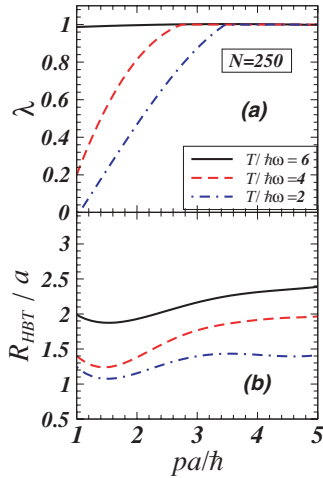


FIG. 7. (Color online) (a) The ratio  $R_{\text{HBT}}/a$  as a function of  $pa/\hbar$  for different temperatures for  $N = 250$ . (b) The parameter  $\lambda$  as a function of  $pa/\hbar$  for different temperatures for  $N = 250$ .

as  $p$  increases. For a fixed value of  $p$  at  $pa/\hbar = 1$ , the HBT radius increases with increasing temperatures very slowly at low temperatures, and it increases rather abruptly when the condensation temperature is approached. For this small value of  $pa/\hbar$ , the variation of  $R_{\text{HBT}}(p, T)$  as a function of  $T$  reflects closely the variation of the root-mean-squared radius as a function of  $T/\hbar\omega$ , as shown in Fig. 4. For large values of  $p$ ,  $R_{\text{HBT}}(p, T)$  increases with increasing temperatures in a more uniform manner.

In Figs. 7(a) and 7(b), we show, respectively,  $\lambda(p, T)$  and  $R_{\text{HBT}}(p, T)$  as a function of  $pa/\hbar$  and  $T$  for the case with  $N = 250$ . The  $\lambda$  parameter and the HBT radius  $R_{\text{HBT}}$  behave in a manner similar to those for the case of  $N = 2000$ . One observes in Fig. 7(a) that at temperatures below  $T_c$ , the  $\lambda$  parameter is small at small  $p$  and it increases as  $p$  increases, reaching the saturating value of unity at  $pa/\hbar = 3.5$  for  $T/\hbar\omega = 2$  and at  $pa/\hbar = 2.7$  for  $T/\hbar\omega = 4$ . Above the condensation temperature at  $T/\hbar\omega = 6$ , the  $\lambda$  parameter assumes the value of unity for all  $p$  values.

As shown in Fig. 7(b), for a fixed value of the temperature  $T$ , the HBT radius  $R_{\text{HBT}}$  decreases slightly and then increases gradually with  $p$ . For a fixed  $p$  with a small  $p$ , the increase in  $R_{\text{HBT}}$  is slow at low temperatures and the increase becomes more rapid as the temperature approaches the condensate temperature of  $T_c/\hbar\omega = 5.12$ .

### VIII. BOSE-EINSTEIN CONDENSATION OF PIONS IN A MEAN FIELD (NON-RELATIVISTIC)

There is not much information on the magnitude of the mean-field potential experienced by the pions. From the Glauber theory [53], the mean-field potential experienced by a pion in a pion medium is related to the pion density  $\rho_r(\mathbf{r})$  by

$$V(\mathbf{r}) = -\frac{2\pi f(0)}{m}\rho_r(\mathbf{r}), \quad (59)$$

where  $f(0)$  is the forward  $\pi$ - $\pi$  scattering amplitude. We hope to evaluate the pion mean-field potential in the future. In the

meantime, the results in the previous sections allow us to answer the following theoretical question: If a system of  $N$  pions is held together by its mean field, taken to be a harmonic oscillator, and if it comes to a state of static equilibrium with a given root-mean-squared radius  $r_{\text{rms}}$  at a temperature  $T$ , what is the condensate fraction of such a system? The answer to this theoretical question will provide useful information on the importance of the Bose-Einstein condensation for a pion system in static equilibrium, to pave the way for future investigations for the system in dynamical expansion.

We would like to examine pion systems with a typical  $r_{\text{rms}}$ ,  $T$ , and pion number that one encounters in high-energy heavy-ion collisions. For a pion gas distribution with an HBT radius of about  $R_{\text{HBT}} = 6$  fm as appropriate for Au-Au central collisions [9], the root-mean-squared radius  $r_{\text{rms}}$  for a Gaussian density distribution is  $\sqrt{3}R_{\text{HBT}}$ , which is about 10 fm. We shall therefore examine a pion system with  $r_{\text{rms}} = 10$  fm, a temperature range from 80 to 160 MeV, and pions numbering  $N = 250$  (for a central SPS Au-Au collision at  $\sqrt{s_{NN}} = 19.4$  GeV) and  $N = 2000$  (for a central RHIC Au-Au collisions at  $\sqrt{s_{NN}} = 200$  GeV).

For a pion with a temperature of 80 to 160 MeV, which is of the order of the pion rest mass of 140 MeV, the motion of the pions is relativistic and the proper treatment will need to be relativistic in nature. We shall carry out a relativistic treatment of the pion states in the next section and shall content ourselves here in the type of solution one gets in a nonrelativistic treatment. Carrying out both relativistic and nonrelativistic treatments will allow one to understand what features of the coherence are sensitively affected by the relativistic motion.

We first determine the strength of the mean-field potential  $\hbar\omega$  that can hold a system of  $N$  pions in static equilibrium at the temperature  $T$  for a given root-mean-squared radius of  $r_{\text{rms}}$ . For the pion system in static equilibrium, the quantity  $r_{\text{rms}}/a$  is a function  $F_N(x)$  of the variable  $x = T/\hbar\omega$  as shown in Fig. 4, where the subscript  $N$  labels the boson number. If the value of  $r_{\text{rms}}$  is fixed as given, the quantities  $\hbar\omega$  and  $T$  are then related by the set of parametric equations

$$\hbar\omega = \frac{[\hbar F_N(x)]^2}{r_{\text{rms}}^2 m}, \quad (60)$$

$$T = x \frac{[\hbar F_N(x)]^2}{r_{\text{rms}}^2 m}. \quad (61)$$

By varying  $x = T/\hbar\omega$  for a fixed  $r_{\text{rms}}$  and using the function  $F_N(x)$  of Fig. 4 in these equations, the energy  $\hbar\omega$  can be determined as a function of  $T$  for the cases of  $N = 2000$  and  $N = 250$ . The results are shown in Fig. 8(a). One finds that for the pion system with a given root-mean-squared radius of 10 fm, the value of  $\hbar\omega$  ranges from about 12 to 20 MeV for  $N = 2000$  and from about 20 to 30 MeV for  $N = 250$ . The ratio of  $T/\hbar\omega$  is about 7 for  $N = 2000$ , and it is about 4.5 for  $N = 250$ , as shown in Fig. 8(b). From these ratios of  $T/\hbar\omega$ , one can use Fig. 2 to find out the condensate fraction. The condensate fractions  $f_0(T)$  for a pion gas at various temperatures with  $N = 2000$  and  $N = 250$  are shown in Fig. 8(c). One finds that  $f_0(T)$  is about 0.67–0.8 for  $N = 2000$  and is about 0.9 for  $N = 250$ . The knowledge of  $\hbar\omega$  in Fig. 8(a) allows one to determine the values of  $a$  as a function of the temperature, as

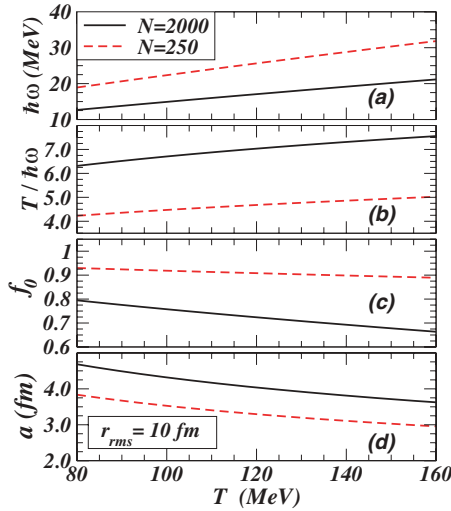


FIG. 8. (Color online) (a) The potential strength  $\hbar\omega$ , (b) the ratio  $T/\hbar\omega$ , (c) the condensate fraction  $f_0$ , and (d) the oscillator length parameter  $a$  for nonrelativistic boson systems with  $N = 2000$  and  $N = 250$  in static equilibrium with  $r_{\text{rms}} = 10$  fm plotted as a function of temperature.

shown in Fig. 8(d). The oscillator length  $a$  is about 4 fm for  $N = 2000$  and about 3.5 fm for  $N = 250$ .

What is the depth of the mean-field potential that holds the pions together in static equilibrium for a given  $r_{\text{rms}}$ ? The depth of the potential is approximately  $\hbar\omega(r_{\text{rms}}/a)^2/2$  [see Eq. (1)]. For  $r_{\text{rms}} = 10$  fm and  $T \sim 120$  MeV, the results in Figs. 8(a) and 8(c) show that the depth of the potential needs to be about  $18(\text{MeV}) \times 2.5^2/2 \sim 56$  MeV for  $N = 2000$ , and it is about  $25(\text{MeV}) \times 3^2/2 \sim 112$  MeV for  $N = 250$ . These are not very deep potentials. It will be of interest to determine theoretically the mean-field potential for an assembly of pions at different temperatures.

We reach the following conclusion from this study: If a nonrelativistic pion system maintains a static equilibrium within its mean field, and if it contains a root-mean-squared radius, a pion number, and a temperature typical of those in high-energy heavy-ion collisions, then it will contain a large fraction of the Bose-Einstein pion condensate. The pion condensation will affect the parameter  $\lambda$  in momentum correlation measurements.

The evolution of pions in high-energy heavy-ion collisions involves dynamical motion and the pions may not be in a state of static equilibrium. The static solutions examined here serve as supplementary tools relative to which the effects of the dynamical motion and nonequilibrium effects may be investigated.

## IX. RELATIVISTIC TREATMENT OF A BOSON GAS IN A HARMONIC OSCILLATOR

For pions in the environment of a high-energy heavy-ion collision, the pion temperature is of the order of the pion rest mass and a relativistic treatment of the pion motion is needed. We therefore examine a boson in an external field characterized by a timelike vector interaction  $A_0(r)$ , a spacelike interaction

$\mathbf{A}(\mathbf{r})$ , and a scalar interaction  $S(r)$ . The Klein-Gordon equation for the motion of the boson is

$$\{[p_0 - A_0(r)]^2 - [\mathbf{p} - \mathbf{A}(\mathbf{r})]^2 - [m + S(r)]^2\}u(r) = 0. \quad (62)$$

Different types of interaction potentials will lead to different single-particle spectra and different Bose-Einstein condensations that will need to be explored in more detail in the future. We shall examine here at this stage only the simplest kind of exactly solvable potential that is closely connected to the harmonic oscillator potential in the nonrelativistic limit. Accordingly, we study scalar interactions  $S(r)$  and introduce the interaction interaction  $V(r)$  related to  $S(r)$  by

$$V(\mathbf{r}) = S(\mathbf{r}) + \frac{[S(\mathbf{r})]^2}{2m}. \quad (63)$$

The  $V(\mathbf{r})$  and the  $S(\mathbf{r})$  potentials approach each other in the nonrelativistic limit of  $m \rightarrow \infty$ . In terms of  $V(\mathbf{r})$ , we have

$$[m + S(\mathbf{r})]^2 = m^2 + 2mV(\mathbf{r}), \quad (64)$$

and the eigenvalue equation for relativistic motion with only a scalar interaction becomes

$$\left[ \frac{\mathbf{p}^2}{2m} + V(\mathbf{r}) \right] u(\mathbf{r}) = \frac{p_0^2 - m^2}{2m} u(\mathbf{r}) \equiv \epsilon u(\mathbf{r}), \quad (65)$$

where the eigenvalue  $\epsilon$  is related to the particle energy  $p_0$  by

$$p_0 \equiv E = \sqrt{m^2 + 2m\epsilon}. \quad (66)$$

To make the problem simple and to connect with earlier exactly solvable nonrelativistic solutions, we choose to consider  $V(r)$  to be the same harmonic oscillator potential of Eq. (1),

$$V(\mathbf{r}) = \frac{1}{2}m\omega^2 r^2. \quad (67)$$

The eigenenergy of the relativistic boson is exactly soluble and is

$$E_n = \sqrt{m^2 + 2m\epsilon_n}, \quad (68)$$

where

$$\epsilon_n = \left(n + \frac{3}{2}\right)\hbar\omega. \quad (69)$$

We likewise introduce the recalibrated  $\tilde{E}_n$  measured relative to the energy of the  $n = 0$  state:

$$\tilde{E}_n = \sqrt{m^2 + 2m\left(n + \frac{3}{2}\hbar\omega\right)} - \sqrt{m^2 + 2m \times \frac{3}{2}\hbar\omega}. \quad (70)$$

Instead of the nonrelativistic condition of Eq. (6), the relativistic condensate configuration condition becomes

$$N = N_0 + N_T = \frac{z}{1-z} + \sum_{n>0}^{\infty} \frac{g_n z e^{-\beta\tilde{E}_n}}{1 - z e^{-\beta\tilde{E}_n}}, \quad (71)$$

where  $g_n = (n+1)(n+2)/2$ .

To solve for the fugacity parameter  $z$  in the relativistic case, it is necessary to specify  $\hbar\omega/m$ , the ratio of harmonic oscillator energy scale  $\hbar\omega$  to the rest mass  $m$  of the boson. A small  $\hbar\omega/m$  ratio approaching zero corresponds to the nonrelativistic limit and a large ratio relative to zero leads to the relativistic case.

We are interested in the case where the mass  $m$  of the boson is of the order of the gas temperature  $T$ . We shall see in Fig. 13(a) later that a boson system with  $N = 2000$  pions,

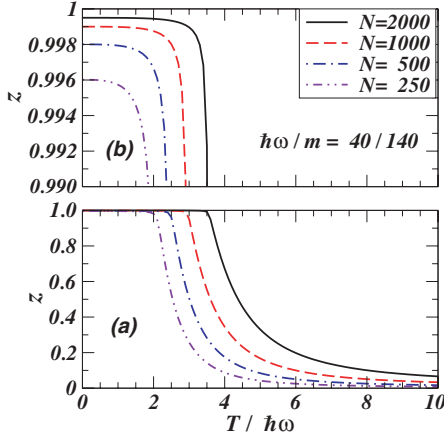


FIG. 9. (Color online) (a) The fugacity parameter  $z$  satisfying the relativistic condensate configuration condition Eq. (71) for different boson numbers  $N$  and  $\hbar\omega/m = 20/140$ , as a function of the temperature  $T/\hbar\omega$  and (b) an expanded view in the  $z \sim 1$  region.

$T \sim m$ , and a root-mean-squared radius of 10 fm corresponds to a harmonic oscillator energy  $\hbar\omega \approx 40$  MeV, which is a substantial fraction of the rest mass  $m$ . We shall therefore investigate relativistic boson systems with  $\hbar\omega/m = 40/140$  in our numerical studies.

With this specification of  $\hbar\omega/m$  with  $N$  and  $\beta\hbar\omega = \hbar\omega/T$  held fixed, the relativistic condensate configuration condition [Eq. (71)] can be solved numerically to determine the unknown  $z$ . We show in Fig. 9 the fugacity  $z$  that satisfies the relativistic condensate configuration condition for different temperatures  $T/\hbar\omega$  and different boson numbers  $N$ . To get a better view of the  $z$  values, we show an expanded view of Fig. 9(a) in the  $z \sim 1$  region in Fig. 9(b).

We observe that the fugacity parameter  $z$  is close to unity in the strongly coherent region at low temperatures. Upon a comparison of Fig. 9 with Fig. 1, one notices that the shapes of  $z$  as a function of  $T/\hbar\omega$  for the relativistic and the nonrelativistic cases are very similar, except that the scale of the temperatures are much reduced for the relativistic case. For  $N = 2000$ , the condensate temperature occurs at  $T/\hbar\omega \sim 3.5$  in the relativistic case, in contrast to the nonrelativistic case at  $T/\hbar\omega \sim 11$ . For  $N = 250$ , the condensate temperature occurs at  $T/\hbar\omega \sim 1.9$  in the relativistic case, in contrast to the nonrelativistic case of  $T/\hbar\omega \sim 5.1$ . To see why these large changes occur, we note that the recalibrated energy expanded in powers of  $1/m$  is

$$\tilde{E}_n = \tilde{\epsilon}_n - \frac{\epsilon_n^2}{2m} + O\left(\frac{\epsilon_n^3}{m^2}\right). \quad (72)$$

For the relativistic harmonic oscillator potential we have chosen, the spectrum of  $\tilde{E}_n$  is nearly the same as those in the nonrelativistic case of  $\tilde{\epsilon}_n$  for small values of  $n$ . However, the spectrum for large values of  $n$  is greatly compressed by the presence of the second term with a negative sign in Eq. (72). As a result, a large number of chaotic particles can be accommodated even at a lower temperature, leading to a large shift of the condensate temperature in units of  $\hbar\omega$  in Fig. 9 when relativistic effects are included.

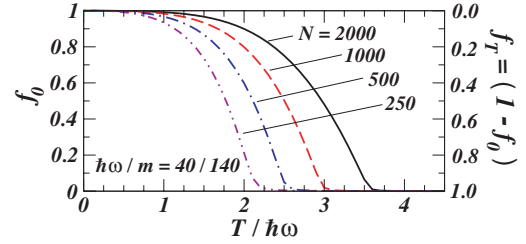


FIG. 10. (Color online) Different curves represent condensate fractions  $f_0(T)$  as a function of  $T/\hbar\omega$  for different boson numbers  $N$ , calculated with the relativistic condensate configuration condition Eq. (71) for  $\hbar\omega/m = 40/140$ . The abscissa labels for the corresponding chaotic fraction  $f_T(T) = [1 - f_0(T)]$  are indicated on the right.

After the value of the solution  $z$  is obtained,  $N_0 = z/(1 - z)$  and  $N_T$  can be subsequently determined to give the condensate configuration specified by the condensate fraction  $f_0$  and the chaotic fraction  $f_T$ .

The condensate fractions  $f_0(T)$  as a function of  $T/\hbar\omega$  calculated with the fugacity parameters of Fig. 9 for different boson numbers  $N$  and  $\hbar\omega/m = 40/140$  are shown as different curves in Fig. 10. The abscissa labels for the corresponding chaotic fraction  $f_T(T) = [1 - f_0(T)]$  are indicated on the right. We observe that the behavior of the condensate fraction in the relativistic case is similar to that of the nonrelativistic case, with the exception of the shift of the temperature  $T/\hbar\omega$  to lower values. Again, the transition from the condensate phase to the chaotic phase occurs over a large range of temperatures and is therefore not a sharp first-order-type transition. The complementary chaotic fraction  $f_T(T)$  increases gradually as the temperature increases, reaching the value of unity at large  $T/\hbar\omega$ .

## X. SPATIAL AND MOMENTUM DISTRIBUTIONS IN THE RELATIVISTIC CASE

Knowledge of the fugacity parameter for different temperatures allows one to determine the occupation numbers at different single-particle states. These occupation numbers and the absolute square of the single-particle wave functions give the spatial and momentum densities of the system at different temperatures. As we remarked previously,  $\rho_p(\mathbf{p})$  and  $\rho_r(\mathbf{r})$  have the same shape when properly scaled. It suffices to consider the spatial density  $\rho_r(\mathbf{r})$  given by

$$\rho_r(\mathbf{r}) = G^{(1)}(\mathbf{r}, \mathbf{r}) = \sum_{n=0}^{\infty} \frac{ze^{-\beta\tilde{E}_n}}{1 - ze^{-\beta\tilde{E}_n}} u_n^*(\mathbf{r})u_n(\mathbf{r}), \quad (73)$$

where  $n$  represents the set of quantum numbers  $\{n_r, l, m\}$  of a harmonic oscillator state,  $u_n(\mathbf{r})$  is the harmonic oscillator wave function normalized to  $\int d\mathbf{r}|u_n(\mathbf{r})|^2 = 1$ ,

$$u_n(\mathbf{r}) = N_{n_r, l} x^l e^{-x^2/2} L_{n_r}^{l+\frac{1}{2}}(x^2) Y_{lm}(\theta, \phi), \quad (74)$$

$n = 2n_r + l$ ,  $x = r/a$ ,  $L_{n_r}^{l+\frac{1}{2}}(x^2)$  is the associated Laguerre

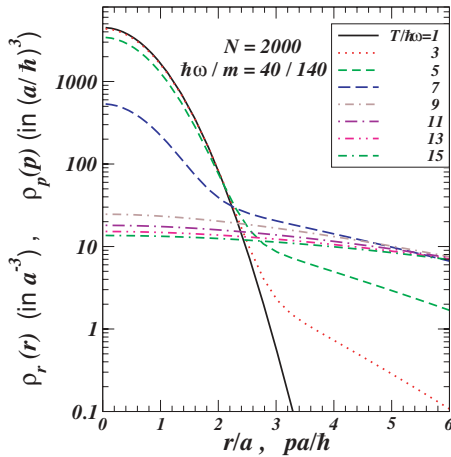


FIG. 11. (Color online) The spatial density distribution  $\rho_r(r)$  in units of  $a^{-3}$ , expressed as a function of  $r/a$ , and the momentum density distribution  $\rho_p(p)$  in units of  $(a/\hbar)^3$ , expressed as a function of  $pa/\hbar$ , for the relativistic case of  $\hbar\omega/m = 40/140$  with  $N = 2000$  at different temperatures.

polynomial, and

$$(N_{n,l})^2 = \frac{2n!}{a^3 \Gamma(n_r + l + \frac{3}{2})}. \quad (75)$$

We plot in Fig. 11 the spatial and momentum distributions of the system with  $N = 2000$  for the relativistic case of  $\hbar\omega/m = 40/140$  as a function of their dimensionless variables  $r/a$  and  $pa/\hbar$ , respectively. One observes that up to  $T/\hbar\omega \sim 3$  the system has a small spatial or momentum size and there is a substantial condensate fraction in the system. In Fig. 12 we plot the root-mean-squared radius in unit of  $a$ ,  $r_{\text{rms}}/a = \sqrt{\langle (r/a)^2 \rangle}$ , and the root-mean-squared momentum in unit of  $\hbar/a$ ,  $p_{\text{rms}}/\hbar = \sqrt{\langle (pa/\hbar)^2 \rangle}$ , as a function of  $T/\hbar\omega$ . For  $N = 2000$ , the quantity  $r_{\text{rms}}/a$  is slightly greater than 1 up to  $T/\hbar\omega \sim 2$ , and it increases relatively rapidly to about 6.5 at the condensate temperature,  $T_c/\hbar\omega \sim 3.5$ . It increases at a relatively slower rate at temperatures above  $T_c$ .

We can carry out an analysis to inquire the following: If a system of  $N = 2000$  relativistic pions is held together by its

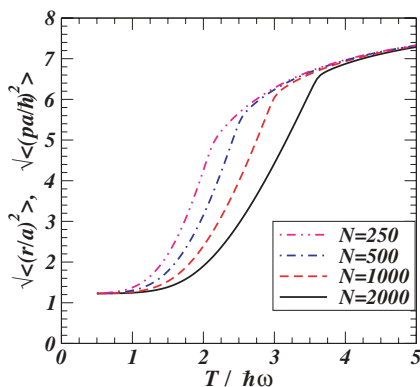


FIG. 12. (Color online) The root-mean-squared radius in units of  $a$  and the root-mean-squared momentum in units of  $\hbar/a$ , as a function of  $T/\hbar\omega$  for different numbers of bosons in the system.

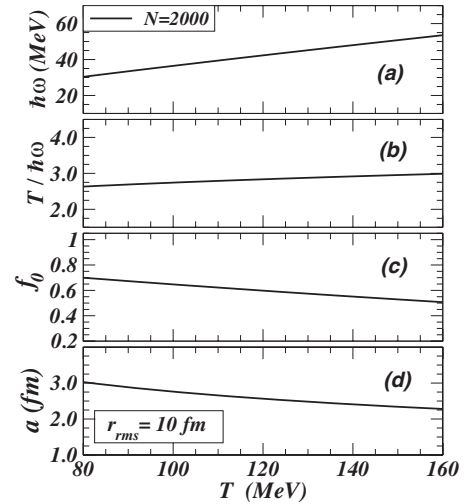


FIG. 13. (a) The potential strength  $\hbar\omega$ , (b) the ratio  $T/\hbar\omega$ , (c) the condensate fraction  $f_0$ , and (d) the oscillator length parameter  $a$  for relativistic boson systems with  $N = 2000$  and  $N = 250$  in static equilibrium with  $r_{\text{rms}} = 10$  fm plotted as a function of temperature.

mean field, taken to be a harmonic oscillator, and if it comes to a state of static equilibrium with a given root-mean-squared radius  $r_{\text{rms}}$  at a temperature  $T$ , what is the condensate fraction of such a system? We shall therefore examine a pion system with  $r_{\text{rms}} = 10$  fm, a temperature range from 80 to 160 MeV, and  $N = 2000$  pions (for a central RHIC Au-Au collisions at  $\sqrt{s_{NN}} = 200$  GeV). We have chosen  $\hbar\omega/m = 40/140$  to be approximately self-consistent with the value of  $\hbar\omega$  extracted from such an analysis [see Fig. 13(a)]. If the value of  $r_{\text{rms}}$  is fixed as given, the quantities  $\hbar\omega$  and  $T$  are then related by the set of parametric equations (60) and (61). Using the function  $r_{\text{rms}}/a = F_N(x)$  of Fig. 12 in these equations and varying  $x = T/\hbar\omega$  for a fixed  $r_{\text{rms}}$ , one can determine the energy  $\hbar\omega$  as a function of  $T$  for the case of  $N = 2000$ . The results are shown in Fig. 13(a). One finds that for the pion system with a given root-mean-squared radius of 10 fm, the value of  $\hbar\omega$  ranges from about 30 to 53 MeV for  $N = 2000$ , with an average of about 42 MeV. The ratio of  $T/\hbar\omega$  is about 2.7 to 3 for  $N = 2000$ , as shown in Fig. 8(b). From these ratios of  $T/\hbar\omega$ , one can use Fig. 2 to determine the condensate fraction. The condensate fractions  $f_0(T)$  for a pion gas at various temperatures with  $N = 2000$  are shown in Fig. 8(c). One finds that  $f_0(T)$  is between 0.5 and 0.7 for  $N = 2000$ . The knowledge of  $\hbar\omega$  in Fig. 8(a) allows one to determine the values of  $a$  as a function of the temperature, as shown in Fig. 8(d). The oscillator length  $a$  is between 3 and 2.2 fm for  $N = 2000$ .

The relativistic analysis indicates that the relativistic effects change the single-particle spectrum and shift the locations of the condensate fraction in units of  $\hbar\omega$ . The condition of maintaining a system size with a root-mean-squared radius of 10 fm recalibrates and raises the oscillator energy  $\hbar\omega$  for the relativistic case, as compared to the nonrelativistic case. As a consequence, the condensate fraction for  $N = 2000$  is modified from  $f_0 \sim 0.67\text{--}0.8$  in the nonrelativistic to  $f_0 \sim 0.5\text{--}0.7$  in the relativistic case. There is a small reduction of

the condensate fraction, but the condensate fraction remains quite large in the relativistic case.

We again reach the following conclusion from this study: If a relativistic pion system maintains a static equilibrium within its mean field, and if it contains a root-mean-squared radius, a pion number, and a temperature typical of those in high-energy heavy-ion collisions at RHIC, then it will contain a large fraction of the Bose-Einstein pion condensate.

## XI. DISCUSSION AND CONCLUSIONS

As the chaoticity parameter  $\lambda$  has been widely used in all HBT measurements, we are therefore motivated to investigate an exactly solvable problem to study the momentum correlation function for a noninteracting boson gas assembly held together in a harmonic oscillator potential at various temperatures. In the process, we find that the phase transition from the Bose-Einstein condensate to the chaotic phase occurs gradually over a large range of temperatures, with the condensate fraction  $f_0(T)$  varying approximately as  $1 - (T/T_c)^3$ , where the condensate temperature  $T_c$  is approximately given by  $(N/1.202)^{1/3}\hbar\omega$ . The spatial and the momentum radii of the system are small in a condensate at low temperatures, of the order of a few oscillator units, increasing in size as the temperature reaches the chaoticity limit.

From the momentum correlation function, we can determine the  $\lambda(p, T)$  parameter and the HBT radius  $R_{\text{HBT}}$ . We find that the  $\lambda(p, T)$  parameter is a sensitive function of both the pair momentum  $p$  and the temperature  $T$ . For a temperature above the condensate temperature, the  $\lambda(p, T)$  parameter is 1 for all momentum  $p$ . However, for temperatures below and even substantially below the condensate temperature,  $\lambda(p, T)$  is small and close to zero for small pair momentum  $p$ , but it increases and saturates at  $\lambda(p, T) = 1$  at large pair momentum  $p$ . The location where  $\lambda(p, T)$  attains unity changes with the temperature. The lower the temperature, the greater is the value of  $p$  at which the  $\lambda(p, T)$  attains the value of unity. Because the  $\lambda(p, T)$  parameter attains the value of unity for systems at temperatures much below the condensate temperature, the occurrence of  $\lambda = 1$  is not consistently correlated with the absence of a condensate fraction. Only in the region of small  $p$  will the parameter  $\lambda(p, T)$  be correlated with, but not equal to, the chaotic fraction  $f_T(T)$  of the system.

We find that the HBT radius  $R_{\text{HBT}}$  increases gradually with increasing pair momentum  $p$  and temperature  $T$ . However, for small value of  $p$ , the HBT radius increases only slowly with increasing temperature at low temperatures and it then increases rapidly and abruptly as the temperature approaches the condensate temperature. The temperature dependence of the HBT radius at small  $p$  values correlates well with the temperature dependence of the root-mean-squared radius of the system.

It is of interest to inquire about the degree of coherence of pion systems produced in high-energy heavy-ion collisions. We have examined both cases of pions as a nonrelativistic and a relativistic gas in a harmonic oscillator potential. If a pion system maintains a static equilibrium in its mean field,

and if it contains pion numbers from  $N = 250$  to  $N = 2000$ , a temperature in the range from 80 to 160 MeV, and a root-mean-squared radius of 10 fm (typical of those one encounters in high-energy heavy-ion collisions), then it will contain a large fraction of the Bose-Einstein pion condensate. The details of the nonrelativistic and relativistic calculations are presented in Secs. VIII and X, but we can provide simple arguments here to indicate that these are reasonable results based on plausible physical principles. Bose-Einstein condensation occurs when the temperature is below the condensate temperature, which is a few units of  $\hbar\omega$ . We need to estimate the energy scale  $\hbar\omega$  for the pion system. The energy scale can be estimated by knowing the length unit  $a$ . One expects that the pion system with a root-mean-squared radius of 10 fm would be contained within a few units of this length  $a$ , leading to a rough estimate of the length unit  $a$  to be about a few femto meters. By dimensional analysis, the energy scale associated with this length unit  $a$  for a pion is  $\hbar\omega = \hbar^2/ma^2$ , which gives a value of many tens of MeV for  $\hbar\omega$ . With a temperature of  $T = 120$  or  $140$  MeV, we obtain the ratio  $T/\hbar\omega$  of a few units, which would correspond to a  $T/\hbar\omega$  ratio with a substantial condensate fraction. We can therefore understand that the occurrence of the pion condensation in static equilibrium arises because the pions are massive particles, and a large number of pions are produced and concentrated in a small spatial volume characterized by a root-mean-squared radius of only 10 fm. The pion gas in static equilibrium is therefore in the realm of low-temperature boson systems with possible occurrence of Bose-Einstein condensation.

The evolution of pions in high-energy heavy-ion collisions contain dynamical motion and may not be in a state of static equilibrium. How the dynamical motion of the pions will modify the coherence of the system will be an interesting subject for future investigations.

While we await future theoretical investigations, it is of interest in the meantime to discuss possible modifications of the static results obtained here in the presence of a collective expansion. One expects that the collective expansion will not alter the energy ordering of the states of the system. Because the Bose-Einstein condensation depends on the relative ordering of the energy of the states, the coherence may not be greatly affected. However, the average pair momentum in the direction of the expansion will be greatly boosted. The  $\lambda(p, T)$  parameter for the expanding coherent source as a function of the pair momentum would likely retain a shape similar to that of the static case, but with the  $p$  boosted by the collective expansion. In this connection, it is interesting to note that the experimental  $\lambda$  values plotted as a function of the pair transverse momentum has a shape [54,55] quite similar to the shape of the  $\lambda(p, T)$  parameter plotted as a function of the average pair momentum  $pa/\hbar$  in Fig. 6(a). Although alternative explanations in terms of a decrease in the resonance decay contributions at higher  $p_T$  have been presented, it will be of interest to explore whether the behavior of  $\lambda$  as a function of the pair transverse momentum may be due to the occurrence of an expanding Bose-Einstein condensate.

The theoretical HBT radius for a static source increases slightly as the pair momentum increases, whereas the experimental measurements give an HBT radius decreasing as  $p_T$

increases. The theoretical HBT radius may be more sensitively affected by the expansion dynamics because the collective expansion boosts not only the average pair momentum but also the relative momentum between the correlated pair, with the boost being greater at larger magnitude of the pion momentum. Because a larger relative momentum leads to a smaller HBT radius, the HBT radius therefore decreases as a function of the pair momentum. Clearly, whether future analyses bear out this possibility will be of great interest. How the collective pion motion will affect quantitatively the HBT radius for a boson system with varying degrees of coherence is therefore an interesting subject for future investigations.

It has been proposed that the question of whether an observation of  $\lambda < 1$  is due to coherence or due to contamination from particles from far outside the source volume can be tested by analyzing three-particle correlations [56]. Such analyses of data at both SPS and RHIC have been consistent with the chaotic conjecture [57]. However, as we note, the  $\lambda(p, T)$  parameter can assume the value of unity in certain kinematic regions even for significantly coherent systems with a temperature much below the condensate temperature, and so the attainment of  $\lambda = 1$  cannot be a unique signature of the chaoticity of a system. However, how the coherence of the boson system may affect three-body correlations has not been worked out explicitly and merits further investigations to clarify the situation.

It needs to be emphasized that to make the problem tractable as an exactly solvable model, we have specialized to a static treatment of the boson system in equilibrium in both a nonrelativistic and a relativistic harmonic oscillator potential, for which analytical eigenenergies and eigenfunctions can be readily available. This is a simple model of a noninteracting boson gas in an external potential without two-body interactions. Even with such an idealization, a wealth of new information on the coherence and two-particle momentum correlation functions as well as the chaoticity parameter has been obtained as a function of the attributes of the boson environment.

The harmonic oscillator potential introduced here can arise from an external trap, as in atomic physics. In high-energy heavy-ion collisions, the harmonic oscillator potential can arise approximately from the mean-field potential experienced by a pion, owing to the interactions generated by other pions and medium particles. Although approximating the pion mean-field potential as a harmonic oscillator potential can yield gross features and a wealth of information, a more accurate determination of the pion momentum and correlation functions will require a better description of the pion mean-field potential. As the mean-field potential depends on the pion density as in the Glauber theory [53], and the equilibrium pion density depends in turn on the mean-field potential, it will be necessary in the future to study the pion mean-field potential and the density self-consistently in a pion condensate. Besides these mean-field interactions between pions, the remaining residue interactions will give rise to additional complications that may be studied in the future.

We have described the correlations in a static equilibrium environment and we need to discuss how the time dependence can be handled. An accurate dynamical treatment

will examine the time evolution of the system for a set of given initial conditions, as in a time-dependent Hartree approximation following the technique of the time-dependent Hartree-Fock approximation developed in nuclear physics. [58,59]

While we await future work on the time dependence of the correlation function, the static results obtained here can be used for experimental comparison if the time dependence of the external field is such that the external potential is suddenly removed, as in a typical condensed matter experiment with trapped atomic particles in a condensate. In these low-temperature measurements with atoms, the trapped atoms before being released are now described as having an equilibrium momentum distribution in momentum space, appropriate for the system in a given external field at a given temperature. The sudden removal of the external field allows the initial momentum distribution of the particle to be frozen at the moment of the external field removal, as appropriate under the application of the sudden approximation in quantum mechanics. Subsequent free streaming of the particles without the external field and mutual interactions (except for the additional correction of the gravitational field or other extra forces applied to the particles) allows the reconstruction of the momentum distribution of the source at the moment of its freezing out. In measuring the arrival times and arrival positions of the particles of a correlated pair in Ref. [50], the quantities that are in effect measured are the momenta of correlated pairs, from which the average momenta and the relative momenta of the pair can be collected and examined. The perspectives of studying the correlation in momentum space presented here offer useful complementary viewpoints to the theoretical and experimental works in atomic physics that have been focused so far on the correlation function in configuration space.

The results obtained here can be approximately applied to heavy-ion collisions if the explosive expansion is so rapid that it can be approximately described as a sudden removal of the external field. In that case, the static initial momentum distribution and correlations of the particles would be frozen at the moment of the external field removal and show up as particles reaching the detectors by free streaming. In this respect, it is of great interest to examine in the future a dynamical model of the expansion of the pion gas and study how the explosive expansion will affect the momentum correlation function.

## ACKNOWLEDGMENTS

The authors would like to thank Prof. R. Glauber for stimulating discussions and for pointing out the importance of the pion coherence in high-energy heavy-ion collisions. The authors wish to thank Drs. Teck-Ghee Lee and Jian-Shi Wu for helpful discussions. This research was supported in part by the National Science Foundation of China under Contract No. 10575024 and in part by the Division of Nuclear Physics, Department of Energy, under Contract No. DE-AC05-00OR22725 managed by UT-Battelle, LLC.

- [1] R. Hanbury-Brown and R. Q. Twiss, *Philos. Mag.* **45**, 633 (1954); *Nature* **177**, 27 (1956); **178**, 1046, (1956); **178**, 1447 (1956).
- [2] For a general review of the Hanbury-Brown–Twiss intensity interferometry, see Chapter 17 of C. Y. Wong, *Introduction to High-Energy Heavy-Ion Collisions* (World Scientific, Singapore, 1994).
- [3] M. Gyulassy, S. K. Kauffmann, and L. W. Wilson, *Phys. Rev. C* **20**, 2267 (1979).
- [4] D. Boal, C.-K. Gelbke, and B. K. Jennings, *Rev. Mod. Phys.* **62**, 553 (1990).
- [5] W. Bauer, C. K. Gelke, and S. Pratt, *Annu. Rev. Nucl. Part. Sci.* **42**, 77 (1992).
- [6] W. A. Zajc, in *Particle Production in Highly Excited Matter*, edited by H. H. Gutbrod and J. Rafelski (Plenum Press, New York, 1993), p. 435.
- [7] U. Heinz and B. Jacak, *Annu. Rev. Nucl. Part. Sci.* **49**, 529 (1992).
- [8] U. A. Wiedemann and U. Heinz, *Phys. Rep.* **319**, 145 (1999).
- [9] M. Lisa, S. Pratt, R. Soltz, and U. Wiedemann, *Annu. Rev. Nucl. Part. Sci.* **55**, 357 (2005).
- [10] G. Goldhaber, S. Goldhaber, W. Lee, and A. Pais, *Phys. Rev.* **120**, 300 (1960).
- [11] G. I. Kopylov and M. J. Podgoretsky, *Yad. Fiz.* **18**, 656 (1973) [*Sov. J. Nucl. Phys.* **18**, 336 (1974)].
- [12] G. N. Fowler and R. M. Weiner, *Phys. Lett.* **B70**, 201 (1977).
- [13] S. E. Koonin, *Phys. Lett.* **B70**, 43 (1977); F. B. Yano and S. E. Koonin, *Phys. Lett.* **B78**, 556 (1978).
- [14] S. Y. Fung, W. Gorn, G. P. Kiernan, J. J. Lu, Y. T. Oh, and R. T. Poe, *Phys. Rev. Lett.* **41**, 1592 (1978).
- [15] M. Biyajima, *Phys. Lett.* **B92**, 193 (1980); *Prog. Theor. Phys.* **66**, 1378 (1981); **68**, 1273 (1982).
- [16] S. Pratt, *Phys. Rev. Lett.* **53**, 1219 (1984); *Phys. Rev. D* **33**, 72 (1986); **33**, 1314 (1986).
- [17] Y. Hama and S. S. Padula, *Phys. Rev. D* **37**, 3237 (1988).
- [18] M. Gyulassy and S. S. Padula, *Phys. Lett.* **B217**, 181 (1988).
- [19] Yu. M. Sinyukov, *Nucl. Phys.* **A498**, 151c (1989).
- [20] D. A. Brown and P. Danielewicz, *Phys. Lett.* **B398**, 252 (1977); *Phys. Rev. C* **57**, 2474 (1998); **64**, 014902 (2001).
- [21] U. A. Wiedemann, B. Tomášik, and U. Heinz, *Nucl. Phys.* **A638**, 475c (1998).
- [22] T. D. Shoppa, S. E. Koonin, and R. Seki, *Phys. Rev. C* **61**, 054902 (2000).
- [23] F. Grassi, Y. Hama, S. S. Padula, and O. Socolowski, Jr., *Phys. Rev. C* **62**, 044904 (2000).
- [24] W. N. Zhang, G. X. Tang, X. J. Chen, L. Huo, Y. M. Liu, and S. Zhang, *Phys. Rev. C* **62**, 044903 (2000).
- [25] M. A. Braun, F. del Moral, and C. Pajares, *Eur. Phys. J. C* **21**, 557 (2001); *Phys. Lett.* **B551**, 291 (2003).
- [26] H. Nakamura and R. Seki, *Phys. Rev. C* **66**, 027901 (2002).
- [27] U. Heinz and P. Kolb, *Nucl. Phys.* **A702**, 269 (2002).
- [28] D. Zschesche, H. Stocker, W. Greiner, and S. Schramm, *Phys. Rev. C* **65**, 064902 (2002).
- [29] C. Y. Wong, *J. Phys. G* **29**, 2151 (2003); **30**, S1053 (2004).
- [30] W. N. Zhang, M. J. Efaaf, C. Y. Wong, and M. Khalilil, *Chin. Phys. Lett.* **21**, 1918 (2004).
- [31] W. N. Zhang, M. J. Efaaf, and C. Y. Wong, *Phys. Rev. C* **70**, 024903 (2004).
- [32] C. Y. Wong and W. N. Zhang, *Phys. Rev. C* **70**, 064904 (2004).
- [33] J. Kapusta and Y. Li, *J. Phys. G* **30**, S1069 (2004).
- [34] W.-N. Zhang, S.-X. Li, C. Y. Wong, and M. J. Efaaf, *Phys. Rev. C* **71**, 064908 (2005); C. Y. Wong, *AIP Conf. Proc.* **828**, 617 (2006).
- [35] O. V. Utyuzh, G. Wilk, and Z. Wdodarczyk, *Phys. Rev. D* **75**, 074030 (2007).
- [36] W. N. Zhang, Y. Y. Ren, and C. Y. Wong, *Phys. Rev. C* **74**, 024908 (2006).
- [37] W. N. Zhang and C. Y. Wong, invited talk presented at the XI International Workshop on Correlation and Fluctuation in Multiparticle Production, Nov. 21–24, 2006, Hangzhou, China, arXiv:hep-ph/0702120.
- [38] C. Y. Wong and W. N. Zhang, invited talk presented at the XI International Workshop on Correlation and Fluctuation in Multiparticle Production, Nov. 21–24, 2006, Hangzhou, China hep-ph/0702121.
- [39] R. J. Glauber, *Phys. Rev. Lett.* **10**, 84 (1963); *Phys. Rev.* **130**, 2529 (1963); **130**, 2766 (1963).
- [40] H. Heiselberg, *Phys. Lett.* **B379**, 27 (1996).
- [41] R. Glauber, *Nucl. Phys.* **A774**, 3 (2006).
- [42] H. D. Politzer, *Phys. Rev. A* **54**, 5048 (1996).
- [43] M. Naraschewski and R. J. Glauber, *Phys. Rev. A* **59**, 4595 (1999).
- [44] J. Viana Gomes, A. Perrin, M. Schellekens, D. Boiron, C. I. Westbrook, and M. Belsley, *Phys. Rev. A* **74**, 053607 (2006).
- [45] M. Yasuda and F. Shimizu, *Phys. Rev. Lett.* **77**, 3090 (1996).
- [46] D. Hellweg, L. Cacciapuoti, M. Kottke, T. Schulte, K. Sengstock, W. Ertmer, and J. J. Arlt, *Phys. Rev. Lett.* **91**, 010406 (2003).
- [47] M. Greiner, C. A. Regal, J. T. Stewart, and D. S. Jin, *Phys. Rev. Lett.* **94**, 110401 (2005).
- [48] S. Fölling, F. Gerbier, A. Widera, O. Mandel, T. Gericke, and I. Bloch, *Nature (London)* **434**, 481 (2005).
- [49] A. Ottl, S. Ritter, M. Kohl, and T. Esslinger, *Phys. Rev. Lett.* **95**, 090404 (2005).
- [50] M. Schellekens, R. Hoppeler, A. Perrin, J. Viana Gomes, D. Boiron, A. Aspect, and C. I. Westbrook, *Science* **310**, 648 (2005).
- [51] J. Esteve, J.-B. Trebbia, T. Schumm, A. Aspect, C. I. Westbrook, and I. Bouchoule, *Phys. Rev. Lett.* **96**, 130403 (2006).
- [52] C. Kittel and H. Kroemer, *Thermal Physics*, 2nd ed. (Freeman, San Francisco, 1980).
- [53] R. J. Glauber, in *Lectures in Theoretical Physics*, edited by W. E. Brittin and L. G. Dunham (Interscience, New York, 1959), Vol. 1, p. 315.
- [54] J. Adams *et al.*, for the STAR Collaboration, *Phys. Rev. C* **71**, 044906 (2005).
- [55] S. S. Adler *et al.* for the PHENIX Collaboration, *Phys. Rev. Lett.* **93**, 152302 (2004).
- [56] U. Heinz and Q. H. Zhang, *Phys. Rev. C* **56**, 426 (1997); U. Heinz and A. Sugarbaker, *ibid.* **70**, 054908 (2004).
- [57] H. Boggild *et al.*, *Phys. Lett.* **B455**, 77 (1999); I. G. Bearden *et al.*, *ibid.* **B517**, 25 (2001); J. Adams *et al.*, *Phys. Rev. Lett.* **91**, 262301 (2003); M. A. Lisa *et al.*, *ibid.* **84**, 2798 (2000).
- [58] P. Bonche, S. E. Koonin, and J. Negele, *Phys. Rev. C* **13**, 1226 (1976).
- [59] C. Y. Wong, J. A. Maruhn, and T. A. Welton, *Nucl. Phys.* **A253**, 469 (1975); C. Y. Wong, T. A. Welton, and J. A. Maruhn, *Phys. Rev. C* **15**, 1558 (1977); C. Y. Wong and J. A. McDonald, *ibid.* **16**, 1196 (1977); C. Y. Wong, *ibid.* **17**, 1832 (1978); C. Y. Wong and H. H. K. Tang, *Phys. Rev. Lett.* **40**, 1070 (1978); *Phys. Rev. C* **20**, 1419 (1979); C. Y. Wong and N. Azziz, *Phys. Rev. C* **24**, 2290 (1981); C. Y. Wong, *ibid.* **25**, 1460 (1982).